Gain Scheduling Control and Loop Interactions in Dual Duct HVAC System

Hanfei Cao

A Thesis

In

The Department

of

Building, Civil, and Environmental Engineering

Presented

In

Partial Fulfillment of the Requirements

for the Degree of Master of Applied Science (Building Engineering) at

Concordia University

Montreal, Quebec, Canada

July 2017

CONCORDIA UNIVERSITY
School of Graduate Studies

This is to certify that the thesis prepared

By: Hanfei Cao

Entitled: Gain Scheduling Control and Loop Interactions in Dual Duct HVAC System

and submitted in partial fulfillment of the requirements for the degree of

Master of Applied Science (Building Engineering)

complies with the regulations of the University and meets the accepted standards with respect to originality and quality.

Signed by the final examining committee:

Dr. H. Ge   Chair

Dr. M.Y. Chen   Examiner

Dr. Z, Chen   Examiner

Dr. M. Zaheeruddin   Supervisor

Approved by

Chair of Department or Graduate Program Director

Dean of Faculty

Date

ii

ABSTRACT

Gain Scheduling Control and Loop Interactions in Dual Duct HVAC System

Hanfei Cao

This research focuses on gain scheduling control of a dual duct system and its local loop interactions. To reach these objectives, experiments were conducted in a dual duct system. The test facility consists three control loops. (cold air temperature control, hot air temperature control, and mixed air temperature control).

The steady state and dynamic characteristics of the dual duct system were studied. Two control strategies were employed to improve the system performance: (i) conventional PI control, and (ii) gain scheduling control. The experimental results subject to load disturbances (set-point changes and initial condition changes) showed that the performance of the gain scheduling controller is better than the conventional PI controller. However, it was found that the gain scheduling control method caused significant oscillations and took nearly 25 minutes to reach a stable final value under low load conditions. Therefore, an adaptive gain scheduling (AGS) controller was developed to improve the disturbance rejection properties of the controller. Experimental and simulation results show that the adaptive gain scheduling controller has dramatically increased controller performance under low load conditions.

The prioritization of control loops due to loop interactions was evaluated and the gain scheduling-adaptive controller was applied to the entire system to minimize loop interactions. The experimental results showed that, compared to conventional PI controller, the dynamic responses of adaptive gain scheduling controller are better.

ACKNOWLEGEMENTS

TABLE OF CONTENTS

LIST OF FIGURES

LIST OF TABLES

NOMENCLRATURE

h_t	*heat transfer coefficient between air and tube* $(w/m^2°C)$
h_{it}	*heat transfer coefficient between tube and water* $(w/m^2°C)$
A	*air sectional flow area* (m^2)
A_{fr}	*face area of the coil* (m^2)
A_o	*total air − side surface area* (m^2)
A_{it}	*tube inside surface area* (m^2)
$\dot{m}_a$	*air mass flowrate* (kg/s)
m_t	*tube mass per unit lenght* $(/m)$
m_{fin}	*fin mass per unit lenght* $(/m)$
m_w	*water mass per unit lenght* $(/m)$
$\dot{m}_w$	*water mass flowrate* (kg/s)
L_c	*coil width* (m)
μ	*dynamic viscosity* $(N * s/m^2)$
k	*heat conductivity* $(\frac{w}{m*k})$
v	*water velocity* $(\frac{m}{s})$
c_{pa}	Specific heat of air at constant pressure $(J/kg°C)$
c_{va}	Specific heat of air at constant volume $(J/kg°C)$
c_w	Specific heat of water $(J/kg°C)$
c_t	Specific heat of tube $(J/kg°C)$
c_{fin}	Specific heat of coil fin $(J/kg°C)$
γ	Specific heat ratio
$T_{a,in}$	Air inlet temperature $(°C)$
Ta_c	Cold duct temperature $(°C)$
Ta_m	Mixed air temperature $(°C)$
Ta_h	Hot duct temperature $(°C)$

$Tchws$	Chilled water supply temperature(℃)
$Tchwr$	Chilled water return temperature(℃)
T_a	Air leaving temperatures(℃)
$\underline{T}_a$	Air mean bulk temperatures(℃)
$\underline{T}_w$	Water mean bulk temperatures(℃)
$\underline{T}_t$	Mean bulk tube wall temperature(℃)
η_s	Fin efficiency
$\eta_{s,ov}$	Overall efficiency
PB	Proportional band
PB_{max}	Maximum value of proportional band
PB_{min}	Minimum value of proportional band
P	Ultimate sensitivity
T	Period of u;timate oosillation (s)
k_p	Proportional gain
$k_{p(max)}$	Maximum value of proportional gain
$k_{p(min)}$	Minimum value of proportional gain
T_i	Integral gain
$T_{i(max)}$	Maximum value of integral gain
e(t)	Error in control variable from its setpoint
$k_1 \& k_2$	Process coefficient
ΔT_{chw}	Chilled water temperature difference(℃)
$\Delta T_{chw,max}$	Maximum value of chilled water temperature difference(℃)

Abbreviations

SSR	Solid state relay
FVSD	Frequency variable speed drive

VM	Valve motor
DM	Damper motor
DAT	Mixed discharge air temperature(℃)
AT_HD	Hot duct air temperature(℃)
CCDAT	Cooling coil discharge air temperature(℃)
AT_inlet	Inlet air temperature(℃)
CHWST	Chilled water supply temperature(℃)
CHWRT	Chilled water return temperature(℃)
CHWF	Chilled water flow rate (kg/s)
GS	Gain scheduling controller
AGS	Adaptive gain scheduling controller
PI	Proportional-integral

equations

$$h_t = m_a * f_1(\frac{1-f_2 m_a^{-1.2}}{1-f_3 m_a^{-1.2}}*(0.0014+f_4 m_a^{-0.4})$$

$$f_1 = \frac{c_p}{A} * Pr^{-2/3} \qquad\qquad f_2 = 1280 N_r (\frac{x_b}{\mu A})^{-1.2}$$

$$f_3 = 5120(\frac{x_b}{\mu A})^{-1.2} \qquad\qquad f_4 = 0.2618(\frac{Dout}{\mu A})^{-0.4} R^{-0.15}$$

$$A = A_{fr} * \frac{\sigma}{4},$$

$$A_{fr} = H * L_c ,$$

$$A_o = V * \alpha,$$

$$A_{it} = \pi * Din * N_r * N_t * L_c$$

$$h_{it} = 0.023 * \frac{k}{Din} * Re^{0.8} * Pr^n \quad \text{note: n=0.3 for heating and 0.4 for cooling}$$

$$Pr_w = \mu_w * c_w / k_w$$

$$Re_w = v_w * Din * \rho_w / \mu_w \qquad\qquad \gamma = \frac{c_{pa}}{c_{va}} = 1.4$$

CHAPTER 1 INTRODUCTION AND LITERATURE REVIEW

1.1 Introduction

HVAC systems are widely used to provide thermally comfortable environments in buildings. The HVAC system is typically designed to deliver conditioned air at the maximum load conditions (designed conditions). However, in most cases, HVAC systems operate at less than full load conditions. This is due to the fact that building loads are dependent on variables which change throughout the day, such as occupancy, ambient temperature, solar load, lights, equipment, etc. Deviation from the design load results in drastic swings or imbalances since the design capacity is greater than the actual load under most operating scenarios. A control system, as well as control schemes and strategies, must therefore be employed to maintain a balance between building loads and heat extraction rates. The improved operation of HVAC systems through controls helps in optimizing a building's energy consumption and ensuring the thermal comfort of the building's occupants.

Due to escalating energy costs, the energy consumption of HVAC systems is facing serious scrutiny. Energy savings in HVAC systems have therefore become a major area of research interest. According to Nabil et al. (2005), most systems in commercial and institutional buildings are not optimized for energy efficiency, which results in energy losses of 15% to 30%. This is tremendous considering HVAC systems can consume up to 30% of the electrical power in buildings. One example of energy waste in the operation of HVAC systems is the simultaneous use of air conditioning and heating, especially in dual-duct systems, which are typically used in buildings.

1

Since building energy conservation has attracted much attention from researchers in the HVAC field, numerous research studies have been conducted in recent decades. Topics such as HVAC systems modeling, dynamic performance, control tuning methods, control strategies, and energy optimization have been studied.

In comparison with experimental research work, model-based simulations have advantages which enable fast and cost-effective designing of HVAC systems. This approach is also able to evaluate system performances under various operating strategies. On the other hand, building or installing a real plant for testing is costly. Model-based simulation is therefore an effective method for research. However, the accuracy of the system modeling must be ensured. To this end, the literature review will focus on the following topics:

1) Modeling of HVAC systems and components
2) Dynamic performance of HVAC systems
3) Controller tuning methods
4) Experimental studies on HVAC control systems

1.2 Modeling of HVAC Systems and Components

Because of the enormous interest in HVAC systems, many researchers have studied dynamic modeling of HVAC systems and their components. The existing system models can be categorized into steady-state models and dynamic models. Generally, steady-state models are used for design. On the other hand, dynamic models describe the dynamics of systems and their components, which are used in system operation and control studies. These models can be grouped into empirical models and lumped capacity models with temporal and spatial variables. The cooling coil is one of the most important components of an HVAC system. As such, several studies have been conducted on the modeling aspects of the cooling coil.

McCullagh et al. (1969) presented a chilled-water cooling and dehumidification coil model. The energy balance equations were applied to air, water, the tube, and the fins. The set of partial differential equations were solved by using the finite difference method. The model considered the dynamic behavior of the coil. However, the experimental results did not show a reasonable match for the small scale coil used in the study.

Clark (1985) developed a cooling and dehumidification coil model based on the steady-state approach presented by Elmahdy and Mitals (1977). The logarithmic mean temperature difference method was used to calculate the heat exchange rate between air and water in the dry case and the wet case respectively. The sensible heat transfer between moist air and water was calculated using the logarithmic mean enthalpy difference method. A time constant was also applied to the steady-state air and water outlet temperatures to develop the dynamic model. However, the model was recommended for small coils (of less than four rows) and the wet coil performance was validated by experiments.

Zheng and M. Zaheeruddin (1997) developed a lumped parameter coil model based on the energy and mass conservation principles. The coil considered several nodes and the properties of

air and water were assumed to be uniform at each node. The dynamics of the air temperature, water temperature, and humidity ratio were described by the ordinary differential equations at each node.

To reduce the complexity of the model caused by the geometric specifications of the coil, Wang et al. (2004) proposed a dynamic cooling coil model based on the energy balance and heat transfer principles with two or three unknown model parameters. The unknown model parameters, such as the chilled water flow rate, air flow rate, and cooling load, were estimated from the real plant commissioning based on the linear least squares method and the Levenberg-Marquardt method. Experiments have been done to verify the model predictions under variable cooling loads. The advantage of the model is the simplification of the cooling coil model due to the coil specification, which could easily be applied to a real plant for real-time control and optimization. However, the model ignores the local loop interactions.

To implement the cooling coil model proposed by Wang et al. (2004), Jin et al. (2006) developed a dynamic model with five model parameters which were determined using experimental data and the manufacturer's catalog. The model was evaluated by the root mean square error (RMS) which showed a proper correspondence between the simulation results and the experimental results. However, real plant applications have not been conducted.

The downside to the cooling coil model is that condensation occurs during the cooling process, which changes the heat transfer coefficient between the air and tubes as well as changing the energy balance from the latent and sensible point of view. To optimize this problem, Yao and Liu (2008) developed a cooling coil model based on the Laplace transform method. The partial-fraction method and Newton-Raphson method were used to transform the transfer function from the spatial domain to the temporal domain. Furthermore the radial basis function neural network (RBFNN) was applied to determine the heat and mass transfer coefficients during the dynamic process. Experiments were conducted for model validation. The results showed that the model with coefficients determined by RBFNN matches the experimental results.

Besides the cooling coil, other components of HVAC systems include supply/return fans, air

ducts, air-conditioning spaces, heating coils, chillers and pumps.

Tashtoush et al. (2004) built an HVAC system model based on energy balance principles which included a zone, a cooling and dehumidifying coil, a humidifier, a heating coil, ductwork, a fan and a mixing box. The Ziegler-Nichols PID method was applied to tune the controller and the trial-and-error method was used to fine-tune the gains.

Zheng and Zaheeruddin (1999) developed a discharge air system (DAT) model which included a coil model, a chiller model, a tank model and a reheat model. The DAT model was optimized by modulating the chilled water flow rate or the hot water flow rate based on a cost function which was numerically solved by the gradient method. The results were presented under the set-point step changes and variable loads.

1.3 Dynamic Performance of HVAC Systems and Components

It is well known that the dynamic performance of the components of an HVAC system has a tremendous impact on the control and energy consumption of the system as a whole.

Robinson (1998) conducted an experiment concerning the damper control characteristics and the temperature stratification in the mixing box. The results demonstrated that the effective control range of the parallel damper was 15° to 60° and the damper position did not significantly affect the mixing effectiveness. However, the effects of the air velocity and its direction were not considered in the study.

Becelaere et al. (2005) conducted an experiment to determine the flow resistance characteristics of the air loop control. Over three hundred and sixty tests were done over a range of operating conditions and system components. The author concluded that the primary influence parameter for the air flow rate was the pressure loss coefficient, which is related to the damper opening position. Other variables included damper type, damper specifications, damper installation, air velocity, blade movement and the total pressure drop in the system.

1.4 Controller Tuning Methods

As stated before, most HVAC systems are operated under partial conditions. Control must therefore be employed to ensure that the system operates efficiently under partial load conditions. Although the dynamic characteristics of the system components have a significant impact on the system control performance, Ruel (2000) concluded that the impact of proper tuning is more important than the components' performance. Because of the importance of the tuning method in control systems research, many tuning methods have been developed in the literature. These methods can be simply classified as either empirical methods, such as the Ziegler-Nichols method and the internal model control (IMC), or analytical methods such as root locus base techniques and methods based on optimization like iterative feedback tuning. In recent years, artificial intelligence techniques such as fuzzy logic, neural networks and genetic algorithms have been studied.

Fruehauf et al. (1994) simplified the IMC-PID tuning rules which were established for general flow and level control loops in process control industries. The simulation results based on the parameter changes showed that the simplified IMC-PID tuning rules were more robust and less sensitive to parameter misestimation compared to Ziegler and Nichols' tuning rules or the Cohen-Coon (1953) tuning rules. They also proposed a new control action – filter action to reduce the measurement and system noise. However, the filter action and derivative action were opposite to each other, which mean both actions could not be used simultaneously. The limitation of this method is that in order to apply the IMC-PID rules, an open loop test must be performed to obtain the process-reaction curve for the dead time and time constant of the system.

To improve the IMC-PID tuning rules' disturbance response, Skogestad, S. (2003) developed a simple IMC-PID tuning method based on the first and second order plus dead time model by using Taylor series approximation to obtain the effective delay time. This method also reduced the complexity of the PID tuning problem to a sole adjustable tuning parameter referred to as the

desired closed loop time constant (τ_c). According to Skogestad, a good trade-off should be obtained between response speed and robustness by choosing the adjustable tuning parameter. The simulation results showed good control performance. However, unstable processes were not examined in the study.

Tuning methods have also been developed based on the constrained optimization techniques by minimizing the integral error criteria, such as the minimum integral of square error (ISE), the minimum integral of absolute error (IAE), the minimum integral of absolute error multiplied by time (ITAE), the total variation (TV) and the sensitivity peak (M_s). Ãstrom and HÃgglund (2004) developed a tuning rule using the M-constrained integral gain optimization (MIGO) method for load disturbance rejection based on the step responses obtained from the Ziegler-Nichols method.

To determine the tuning parameters, Ãstrom and HÃgglund determined a set of controller parameters by varying the specified design parameter M_s. A value of $M_s = 1.4$ was recommended for good performance and robustness for the first-order processes. However, the tuning method did not consider the set-point changes or input/output noise effects.

John et al. (2012) proposed a new PID tuning strategy for a discharge air temperature system which aimed to attenuate the overshoot. The tuning method was based on the first-order system with time delay. According to John et al., the PI tuning could be reduced to one-dimensional tuning by adjusting only the proportional gain, which would reduce the tuning complexity and enhance control robustness. Based on the simulation results, the proportional gain value for a discharge air temperature system could be identified as the following equation:

$$\frac{k_p}{k_s} = \frac{0.855 + 0.002035 * (T+\tau) + 65.5}{T+\tau}$$

However, the system capacity and proportional gain values are limited in the study due to the limitations of the first-order system model.

Lin et al. (2008) conducted a comprehensive study to compare ten recently popular tuning rules based on their performance under different operating conditions. The comparison was based on

the integral absolute error (IAE), total variable (TV) and maximum sensitivity (Ms). A case study on a gas-fired heater was also conducted for the purpose of comparing the results. According to Lin et al., Huang and Jeng's (2003) rules were recommended in the case of a noise free servo control problem with a rapid servo response. However, for a noisy servo control system, Skogestad's rules should be the first consideration for satisfactory output performance. Moreover, for a regulatory problem, Ãstrom and HÃgglund's rules were the first choice for a noise-free system, and Skogestad's rules are more suitable for noisy systems.

To explore the possible causes of hunting in the variable air volume (VAV) system, Yamakawa et al. (2009) developed a dynamic bilinear system model with time delay feedback. The magnitudes of the set-point value, initial value and dead time were considered as the factors that cause the hunting. According to Yamakawa et al., the values of set-point strongly influence the system stability. Simulation results show that the system starts with a small oscillation as the set-point decreases until the hunting begins as the set-point limit is reached. However, the set-point limit of P- action is larger than that of PI- action. Moreover, the dead time also affects the system stability. Based on the simulation results, it was noted that as the dead time becomes larger, the control parameters become very small in the bilinear system.

1.5 Experimental Studies on HVAC Control Systems

Jette et al. (1998) conducted an experimental study on a variable air volume dual duct HVAC system to test the control performance of the system under different tuning methods. The tuning methods studied were Ziegler and Nichols' tuning rules, the simplified IMC-PID tuning rules and Bekker et al.'s tuning rules. These tuning rules were applied on different control loops of the VAV system such as the fan control loop, the damper control loop, the cooling coil valve control loop and the heater control loop. The experimental results showed that Ziegler and Nichols' tuning rules were better for slow time scale systems such as valve control and heater control systems. On the other hand, the simplified IMC-PID tuning rules were better for fast time scale systems like the fan and damper control systems.

The study also investigated the interactions occurring among the four control loops through simulation of a poorly tuned controller. The simulation results indicated that several interactions occur between the valve and the damper control loop and the damper movement impacts the fan speed control. The interactions between the control loops were found to be severe under partial load conditions and minimal under full load conditions.

Matusu and Prokop (2010) conducted an experimental verification of nine conventional PI/PID controller design methods. The controllers were tested using simulations and then implemented under real conditions. The results from the simulations and the experiments were compared. A controller was used to control the airflow speed in a laboratory hot air tunnel model. The step response method was used to identify the plant process function as a second-order process transfer function and a first order plus dead time process transfer function. By comparing the results, Matusu claimed that the balanced tuning of the PI controller performed the best with the lowest overshoot and the Chien-Hrones-Reswick, Fruehauf (1994) desired model method give the lowest ISE. However, the experimental tests were limited to systems with fast time scale processes such as fan speed control.

Warren et al. (2009) conducted an experimental study on the energy balance uncertainty analysis caused by the sensor's accuracy. The experimental results showed that high accuracy instruments and proper installation have a negligible effect on energy balance performance. However, when using low accuracy instruments, a large error was noted in the energy balance test. To check the accuracy of the temperature sensors, operational tests were conducted. For the water temperature sensor test, all fans were shut down and only water was circulated through the system for several hours. Similarly, for the air temperature sensor, all water pumps were shut down and only air was distributed through the system. It was noted that all the readings from the temperature sensors were within the accuracy of $0.25℉ (0.14℃)$, which corresponded with the manufacturer's specifications.

10

1.6 Objective of Research

From the literature review presented above, it can be noted that most of the experimental studies have focused on the application of tuning rules on single control loops at the component level. Experimental control system research on entire HVAC systems with multiple control loops is lacking, with the exception of the study by Jette et.al (1998). It is also noted that the study of gain scheduling control in HVAC systems has not been explored. With this as the motivation, an experimental study of gain scheduling control of a multiple control loop dual duct HVAC system is proposed in this thesis. This research will mainly focus on the dynamic performance of HVAC systems and adaptive control design to improve control performance of a dual-duct system.

The main objectives of the research proposed in this thesis include:

1. To install and commission an existing dual duct HVAC system. The installation includes adding a new chiller system and reconfiguring the control loops with new sensors, actuators and Honeywell's Building Automation System.
2. Conduct steady-state and dynamic response tests on each of the following control loops one at a time: (i). Cool air temperature control loop, (ii). Warm air temperature control loop, and (iii). Mixed air temperature control loop. Also, study the steady-state and dynamic responses of the whole dual duct HVAC system with multiple control loops.
3. Design a gain scheduling PI control strategy and test the system performance under gain scheduling PI control. Compare the control performance of the system with PI control and the gain scheduling PI control.
4. A load-following adaptive gain control strategy will be proposed to improve the control performance of the dual duct system.
5. To evaluate and minimize the interaction effects between the control loops under adaptive gain scheduling PI control and the conventional PI control.

To achieve these objectives, a dual duct HVAC experimental facility was commissioned. The system consists of a chiller, a cooling coil, a supply fan, two electric heaters, two dampers and

one mixing chamber. Three control loops will be studied in this research and all control variables will be controlled by a Honeywell controller based on a Tridium platform.

CHAPTER 2   SYSTEM DESCRIPTION

2.1 Introduction

An existing dual duct HVAC system test facility in Concordia University's Building Engineering Lab is recommissioned by installing a new chiller system, sensors, actuators and Honeywell's Building Control System. The test facility is recalibrated and reconfigured with new control hardware and software to conduct control systems experiments. The test facility will be described for both mechanical systems and control systems. The mechanical system components consist of a cooling and dehumidifying coil, a chiller, two main ducts, an air mixing chamber, a water flow control valve, an electric heater, an air supply fan and dampers. The control system includes control software from Honeywell as well as controllers, sensors and actuators. There are three local control loops that will be studied in this thesis:

1. A cold air temperature control loop
2. A hot air temperature control loop
3. A mixed air temperature control loop

2.2 Mechanical System

The schematic diagram of the dual duct HVAC system test facility is shown in Figure 2.1. It consists of a supply fan equipped with a variable D/C motor, two electrical heating coils, a chilled water cooling and dehumidifying coil, two main ducts, a mixing box and a mixed air duct. The two main ducts are respectively equipped with an electrical heating coil and a chilled water cooling and dehumidifying coil, which are used to heat or cool the air at the desired set-points. A supply fan is used to drive the airflow into the system, and an electrical heating coil is

installed on the supply fan intake to create cooling load. Two dampers are used for modulating the airflow to the mixing box to obtain a desired discharge air temperature.

As the system is installed indoors, the room temperature air is heated by the electrical heater to create a load. The warm air enters the dual-duct system. The airflow is then divided into two streams, one leading to a cool air duct and the other to a warm air duct. One part is heated by the electrical heater to a set-point temperature by modulating the power input. The other part is cooled by the cooling coil by modulating the chilled water flowrate. The cold-air duct and the hot-air duct are insulated up to the mixing box to reduce heat losses and heat gains from the ducts. The mixed air temperature is controlled by modulating the damper in the hot-air duct while the damper in the cold-air duct is kept fully open during the entire operation.

The physical system is connected to a PC for monitoring and control purposes. An overview of the control system is given as the following figure.
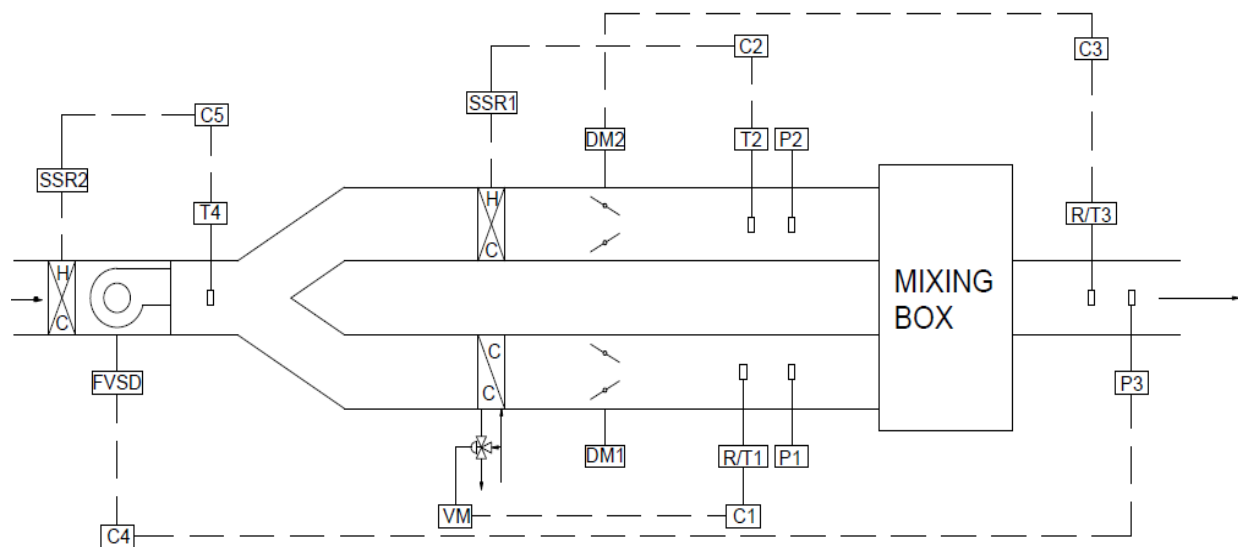
Figure 2.1Schematic diagram of the dual duct HVAC test facility

Note: The legends of the diagram are shown in the following table

14

Symbol	Description
SSR	Solid state relay
FVSD	Frequency variable speed drive
HC	Heating coil
CC	Cooling coil
T	Temperature sensor
R/T	Humidity/temperature sensor
P	Air flow sensor
VM	Valve motor
DM	Damper motor
C1 – C5	Controllers

2.2.1 Cooling and Dehumidifying Coil

The selected cooling coil has a capacity of 12,000BH (3,417W) with five rows (12 fins per inch). The measured dimensions of the coil are 12''x 12'' x 4'' (length, height, and thickness). The chilled water passes through the coil in a counter-flow mode, which is known to give higher efficiency since it has higher overall temperature differences between the air and water throughout the heat exchanger. The chilled water is supplied by the refrigeration system.

2.2.2 Refrigeration System

The refrigeration system is an M1-2W mode 2-ton chiller which was manufactured by Advantage Inc. It includes an internal pumping system and a reservoir system. The chiller uses mechanical refrigeration to cool the water within the range of 20°F(−6.7°C) to 70°F(21.1°C). It provides 2 tons of refrigeration and uses R410A as the refrigerant. City water stored in a reservoir is used to dissipate the heat from the refrigeration system. There is an automatic control panel on the chiller to control the water temperature by modulating the refrigerant flow rate in

the system.

2.2.3 Chilled Water Flow Control Valve

The chilled water flow control valve is a Belimo three-way valve with ½ inch connections. It has a flow coefficient of Cv=1.9gpm/psi. The valve is equipped with a proportional controlled actuator. It is used for regulating the valve position, thereby modulating the chilled water flow rate to adjust the cold air discharge temperature at the setpoint. For example, during the operation of the system, as the cold air discharge temperature is higher than the set point, the three-way valve is fully opened and thereby the chilled water flows into the cooling coil to cool the air. As the discharge air temperature reaches the set-point, the three-way valve is modulating its position to control the chilled water flow rate and thereby the discharge air temperature.

2.2.4 Electrical Heaters

Heating of the air is performed by the electrical heaters. There are two electrical heaters in the system. One is used to heat the room air at the fan intake to create a load which has a capacity of 6 KW. The other heater, which has a capacity of 2400W under 240V power input, is used as a heating coil to heat the air to a desired temperature in the hot air duct. The heaters are controlled by the controller through a solid state relay (SSR) device which works by time proportioning the power to the electrical heater. This action essentially provides continuously variable heat output to meet the exact needs of the system.

2.2.5 Supply Fan

A backwards inclined centrifugal fan is equipped in the test facility to supply air to the dual-duct HVAC system. The fan speed ranges from 360 rpm to 1600 rpm, which can provide an average flow rate of 860 cfm under a power input of 0.21 HP.

The fan speed is varied by the variable frequency speed drive to maintain a constant velocity and pressure in the mixed air duct.

2.2.6 Dampers

There are two dampers in the system: one in the hot duct and one in the cold duct. Each damper measures 12in. X 12in. The dampers are of the opposed blade type which provides a more uniform flow compared with parallel blade dampers. During operation, the damper in the cold duct is kept fully open and the damper in the hot duct is modulated to control the mixed air temperature.

2.3 Control System

The control and data acquisition functions are implemented in a windows-7 based PC platform. A BACnet interface is used to communicate between the PC and the controllers. A Honeywell Spyder controller and a Honeywell Sylk I/O device are used for communicating between the computer and the control hardware system. The Honeywell Spyder controller has six analog inputs and three analog outputs and the I/O device has six analog inputs and four analog outputs which carry the system inputs to the PC and the outputs to the system. The sensors and actuators are all wired and configured to the controller based on the product specifications. The control and monitoring system performs the following functions:

- PID tuning and control
- Data acquisition and processing
- Monitoring of operating points and control action
- Programming environment for implementation of control strategies

The controller is a programmable controller with a graphical environment. It is supported by the Honeywell Spyder workbench which provides the programming environment for the Honeywell Spyder controller. The Honeywell Spyder workbench is based on Niagara AX framework by Tridium.

During the operation, the controller receives the current signal from the sensors and the current signal is converted into a readable format by the workbench as the inputs. As the control

17

algorithm is created in the control tool as a graphical framework, the inputs are used to calculate the control parameters and stored for research analysis. Once the control parameters are calculated, output voltage signals are sent to the actuators for control purposes.

There are five local control loops in the system. The following is a brief description of the control loops.

2.3.1 Description of the Control Loops

Loop 1: Cold Air Temperature Control Loop

The cold air temperature is controlled by modulating the chilled water flowrate through a three-way valve. The control loop (Figure 2.2) consists of a cooling and dehumidifying coil, a three-way valve, a valve motor and a refrigeration system. The humidity and temperature sensors measure the air temperature T1 in the cold duct and send a current signal to the controller C1. The controller C1 compares the temperature T1 with the set-point temperature Ts1 which creates an error signal. The error signal is used to generate the control signal by C1, which then sends a voltage output signal to the chilled water three-way valve motor actuator. The motor actuator adjusts the valve position to maintain the cold air temperature at the desired set-point Ts1.
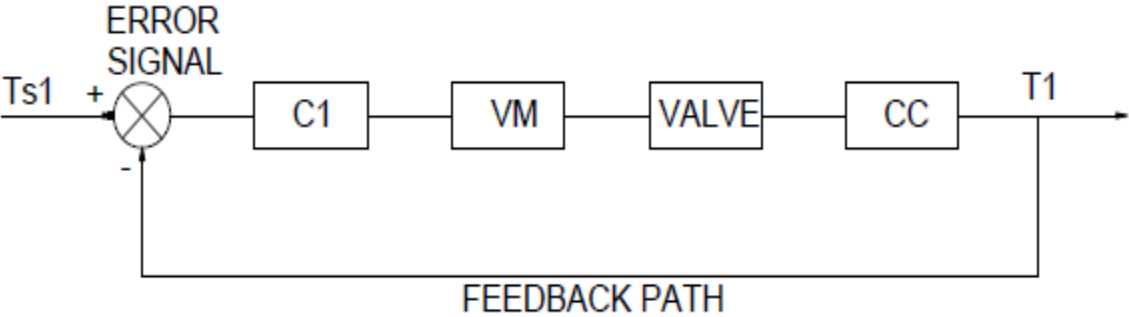
Figure 2.2 Cold air temperature feedback control loop

18

Loop 2 & 3: Hot air temperature control loop

The hot air temperature is controlled by modulating the power input to the electrical heater. The control loop (Figure 2.3) consists of a heating coil and a solid state relay device. Controller 2 compares the discharge air temperature T2 with the set-point temperature Ts2 and generates an output signal which is sent to the solid-state relay device SSR1. The SSR1 relays time proportioning power input to the electrical heater which essentially provides a continuously variable heat output to maintain the hot duct temperature at its desired set-point.
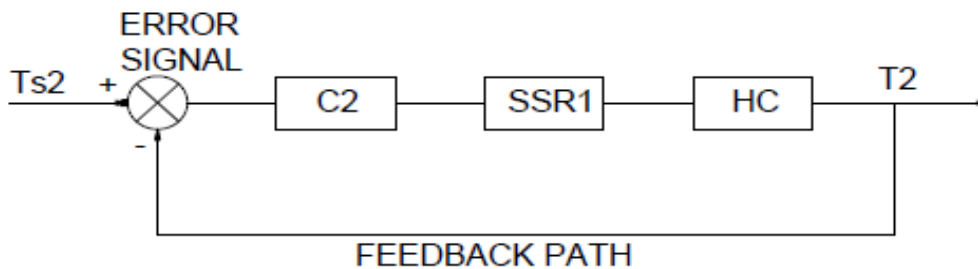
Figure 2.3 Hot air temperature feedback control loop

There is another heating control loop at the supply fan intake to simulate the cooling load for the system. In this case (Figure 2.4), the power input to the electrical heater is controlled by the SSR2 with a signal from the controller to maintain the desired intake air temperature.
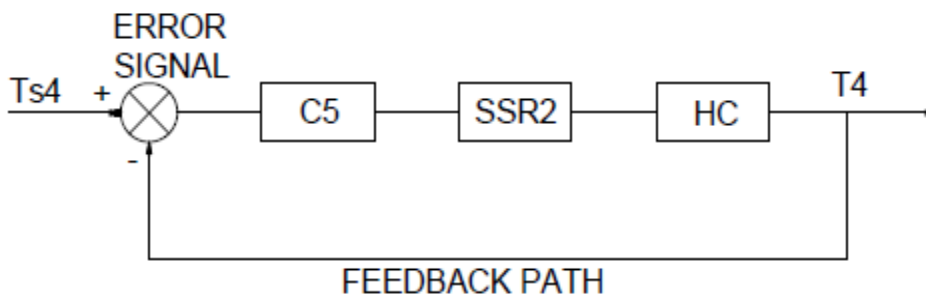

Figure 2.4 Intake air temperature control loop

Loop 4: Mixed air temperature control loop

The mixed air temperature is controlled by modulating the damper position in the hot air duct, and thereby the hot air flowrate is controlled to maintain the mixed air temperature at the set-point. The feedback control diagram for the mixed air temperature control loop is shown in Figure 2.5. As shown in the figure, the mixed air temperature is maintained at its set-point Ts3 by modulating the damper position.
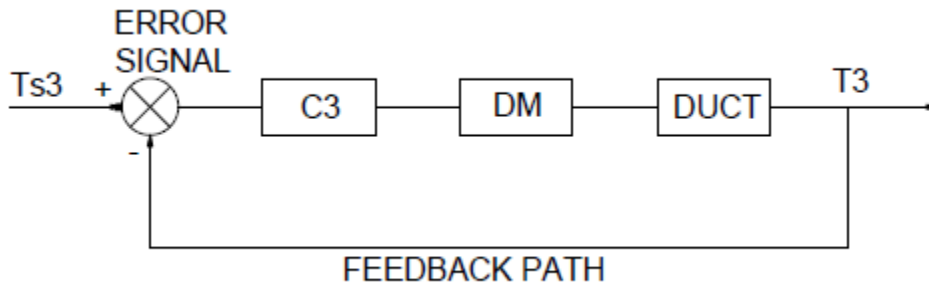
Figure 2.5 Mixed air temperature control loop

Loop 5: Fan speed control loop

The purpose of the fan speed control loop is to maintain a desired air flow rate (static pressure) at the mixed air duct by varying the fan speed. The control loop (Figure 2.6) consists of a centrifugal fan and a variable frequency drive. The details regarding the fan speed control loop components are given in Jette et.al (1998). In figure 2.6, the differential pressure flowmeter measures the flow rate in the mixed air duct which is compared with the set-point Ps. The controller output is then sent to the variable speed drive, which modulates the fan speed in accordance with the pressure set-point.
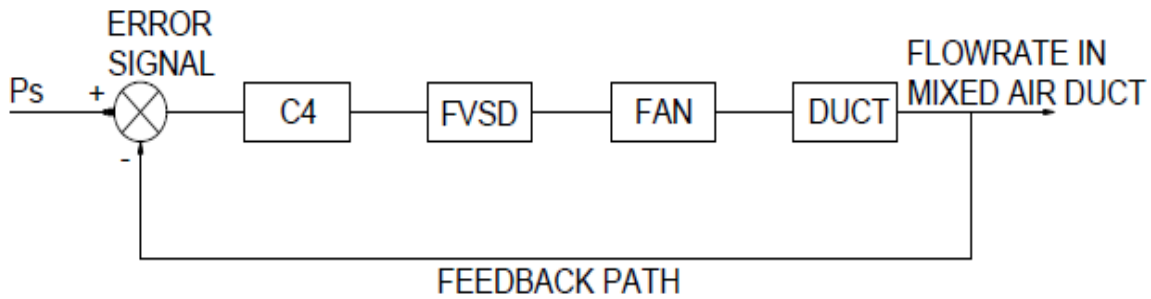
Figure 2.6 Fan speed feedback control loop

2.3.2 Sensors

Temperature sensors, humidity sensors and differential pressure flow sensors are installed in the dual duct system. The installed sensor locations are depicted in Figure 2.1.

a. **Temperature sensors**

The temperature sensors used are C7041 series electronic temperature probe sensors from Honeywell, which are recommended for measurement of discharge air temperature in the ducts. There are two temperature sensors in the system, one in the downstream of the mixing box and another one in the heating coil. The operational range of the temperature sensor is from -40℃ to +121℃ with an accuracy of ±0.25℃ at 25℃.

To determine the accuracy of the temperature sensor, a VELOCICALC multi-function ventilation meter with an accuracy of ±0.1℃ was used for the calibrations. The experiments were conducted to collect the temperature data from the sensors and compare them with the manual readings obtained from the more accurate temperature meter. The manual readings are taken every 10 seconds over a period of 3 minutes. The sensor readings are recorded automatically by the control software with a 5 second interval. Figures 2.7 to 2.10 show that the maximum temperature difference between the readings from the sensors and the velocicalc multi-function ventilation meter is ±0.15℃, which is within the accuracy range of

the sensors.
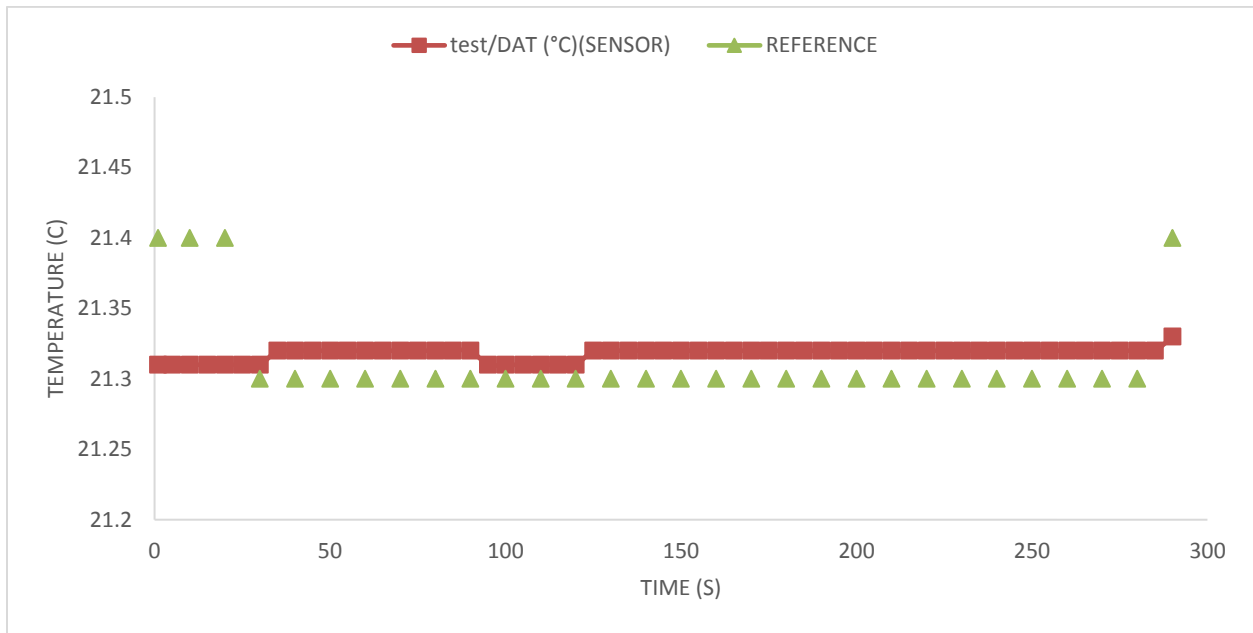
Figure 2.7 Mixed air temperature sensor calibration
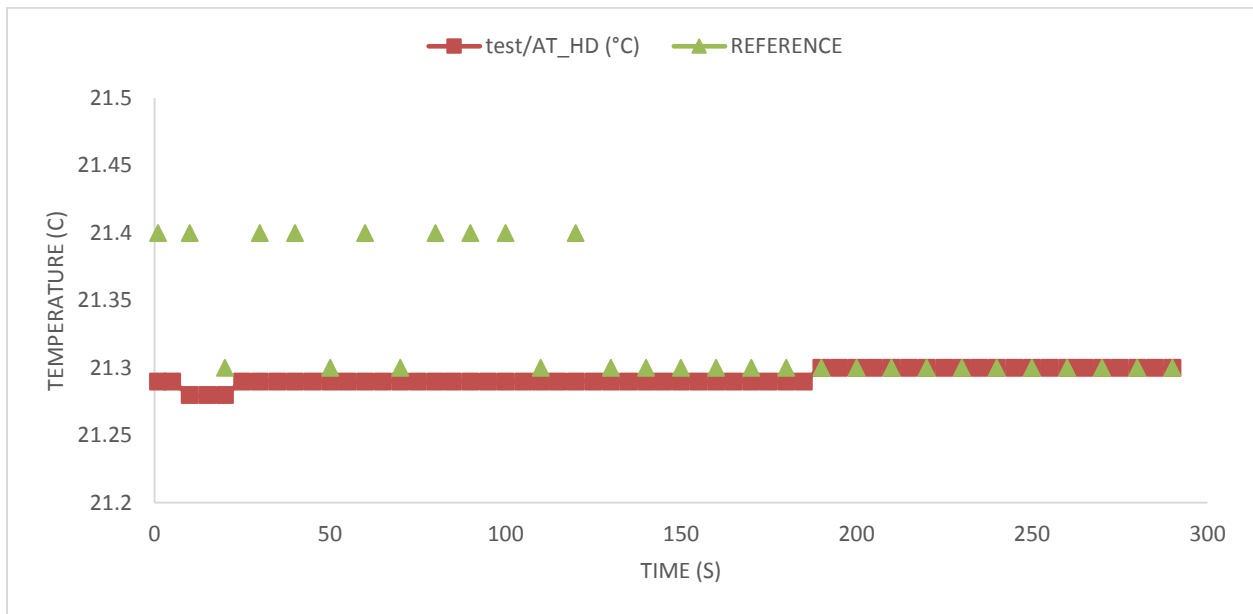
Figure 2.8 Hot-duct air temperature sensor calibration

22
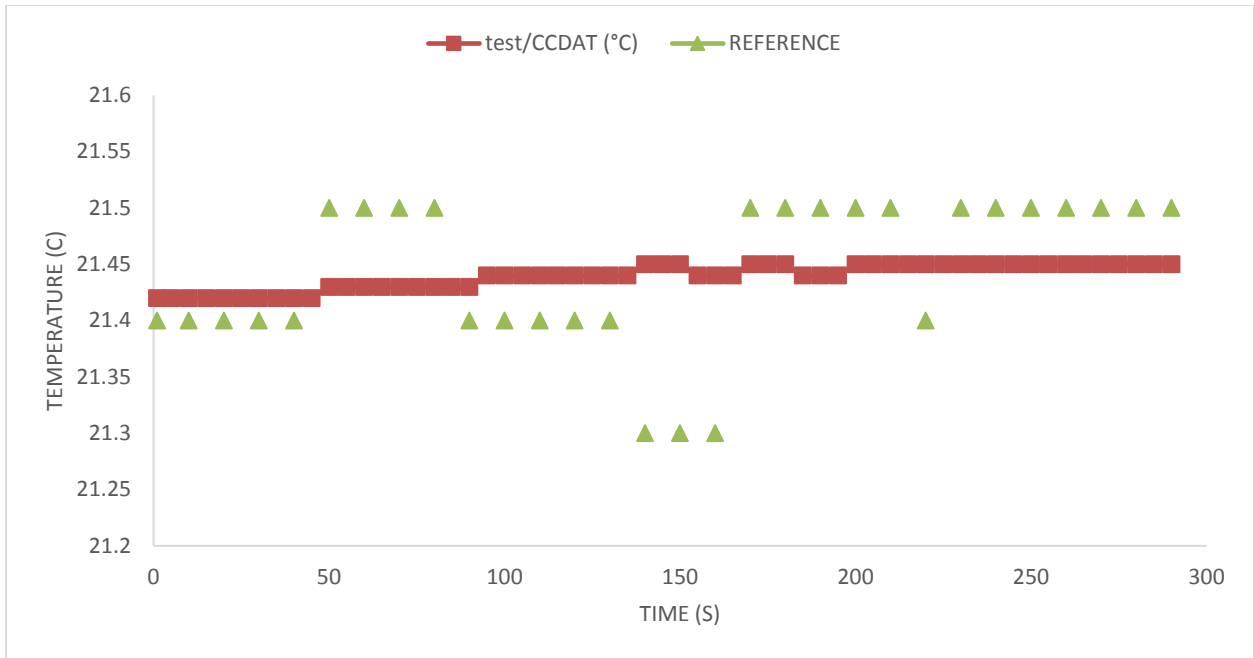
Figure 2.9 Cold-duct air temperature sensor calibration
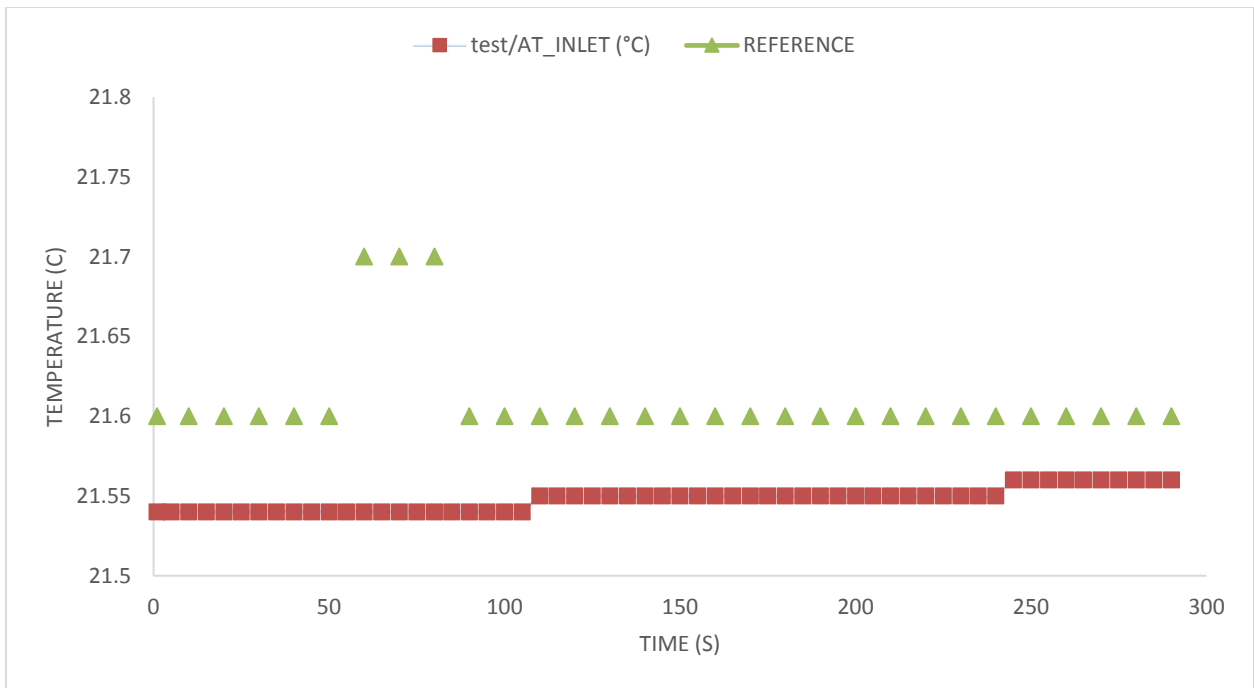
Figure 2.10 Inlet air temperature sensor calibration

23

b. Humidity and temperature sensor

The chosen humidity and temperature sensor is a series 2000 sensor from Honeywell with high accuracy and stable operation. There are two humidity and temperature sensors in the downstream of the cooling coil and the supply fan, respectively. The humidity sensors' operational range is 0 to 95% without condensation. The accuracy of the humidity sensor is $\pm2\%$. The output range for the temperature sensor is -40℃ to 116℃ with an accuracy of ±0.25℃ at 25℃.

To determine the accuracy of the humidity sensor, a VELOCICALC multi-function ventilation meter with an accuracy of $\pm1\%$ was used for the calibrations. The experimental data was collected from the humidity sensor and compared with the manual readings from the humidity meter. Figure 2.11 shows the results of the comparisons. The maximum humidity difference between the sensors and the VELOCICALC multi-function ventilation meter is $\pm1.1\%$. This is within the humidity sensor's tolerant accuracy range.
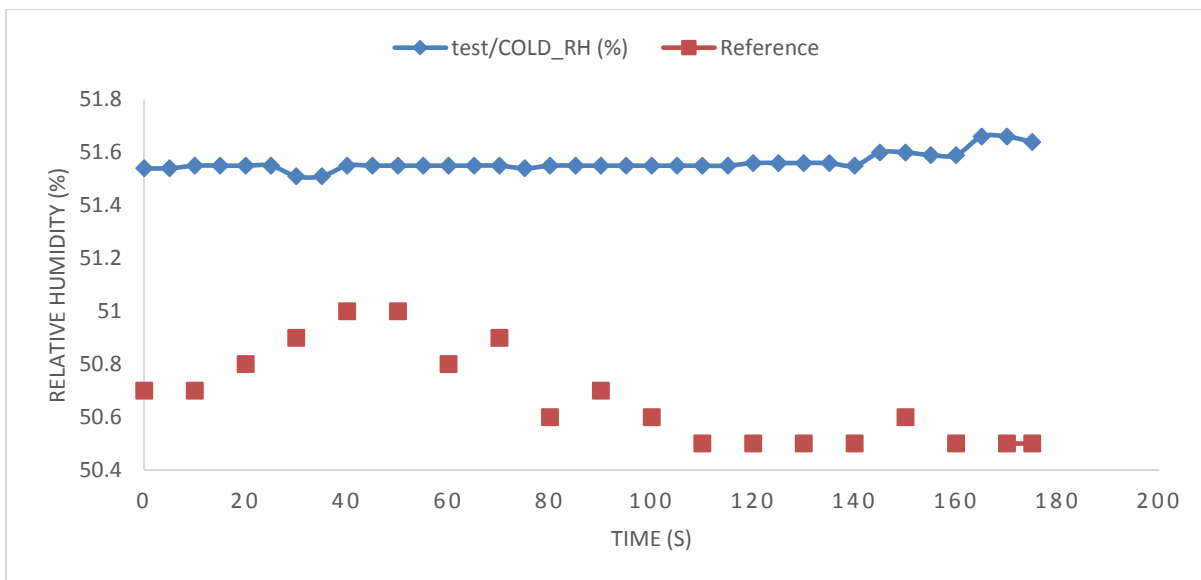
Figure 2.11 Relative humidity sensor calibration

c. Differential pressure flow meter

The AD-1251 probe with differential pressure transducer was used for airflow measurement and fan speed control. The probe is a differential air pressure measuring device that measures

24

the air velocity of the airflow, which corresponds to the airflow rate according to the pressure across measuring system (PAMS) chart. The standard 0 - 10 Volt transducer output signal is proportional to the airflow rate (CFM) and routed to the controller for fan speed control. The differential pressure probe flowmeter measures the airflow effectively for speeds ranging from 400 fpm to 5000 fpm with an accuracy of $\pm 5\%$.

The differential pressure flow meters were also calibrated by using a Dwyer pressure transmitter with an accuracy of 0.001-inch WG. The trials were conducted for different fan speeds. The input of the differential pressure flow meter is the pressure in inch WG which is converted into the airflow rate (CFM) by the following equation according to the PAMS chart:

$$CFM = A_c * K_a * PAMS^{l/m}$$

Where

A_c is the cross section area of the duct

K_a=3493, which is the flow constant varies by the probe type and dimension

$\frac{l}{m} = 0.551$

The air flow rate data is recorded by the control software automatically with a 1 second interval over the duration of 3 minutes. The average value is calculated to eliminate the small fluctuations.

The accuracy of the pressure flow meter is verified by the Dwyer micro-manometer with an accuracy of$\pm 5\%$ in WG. The pressures are measured by the micro-manometer at the outlet of the mixed air duct while the flow is stable. The airflow rate was then calculated by the following equation:

$$CFM = A_c * \sqrt{P} * 4005$$

Where,

A_c is the cross section area of the duct

P is the pressure in inch WG.

Figure 2.12 and 2.13 show that the maximum flow rate difference between the pressure

differential flow meter and the Dwyer micro-manometer is 70 cfm in the cold duct under a low flow rate of 270 cfm. The difference may be caused by the low accuracy of the pressure differential flow meter under low velocity (minimum effective velocity is 400 fpm). There is an error of 7.5% within the effective velocity in the cold duct. The error is also probably due to the air leakage in the cold duct since the error in the hot duct is within the tolerant range.
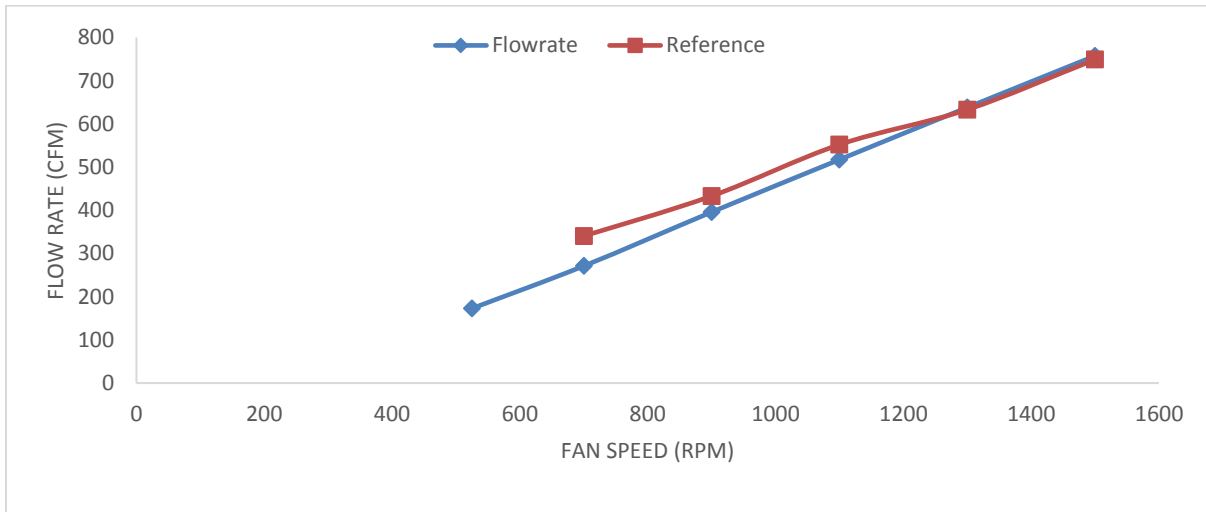
Figure 2.12 Cold-duct airflow rate calibration
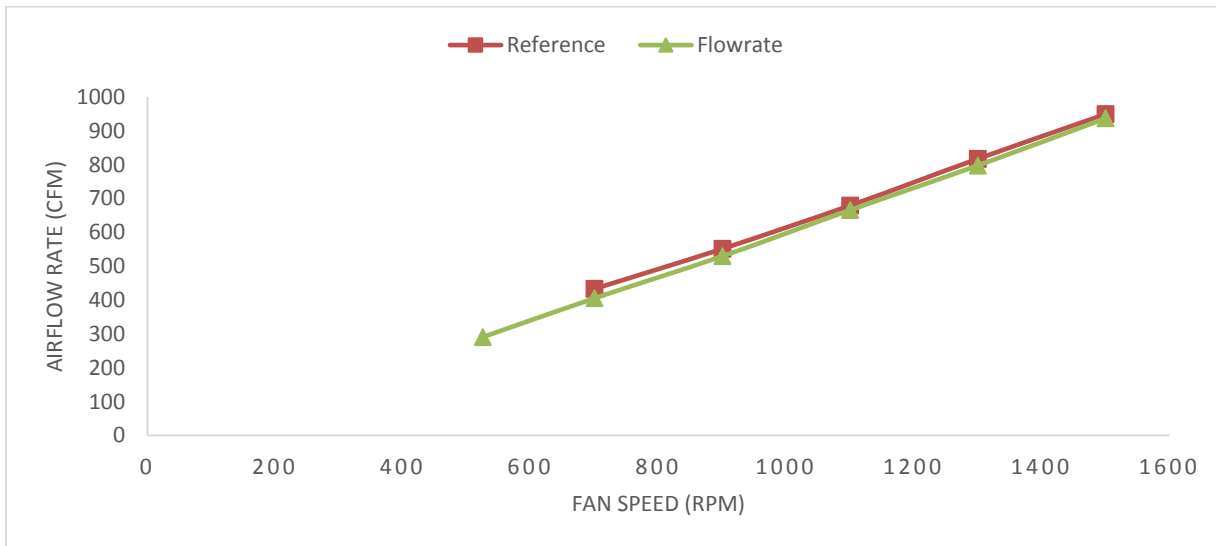
Figure 2.13 Hot-duct airflow rate calibration

d. Water flow meter

The chilled water flow meter used is an OMEGA FMG80A series low flow mag-meter. The measuring range of the flow meter is from 0.2gpm (cut off) to 20 gpm with an accuracy of±1% and ±0.002gpm. The flow meter is fed by a 10-15 VDC power. Once the flow meter is powered on, it generates one pulse to the controller for the corresponding water flow rate. However, the flow meter should be filled with fluid during normal operation, as otherwise a time delay will occur at the start of the data acquisition phase.

2.3.3 Actuators

The experimental facility employed two damper actuators for the damper control, two solid-state silicon rectifiers (SSR) for the electric heater control and one valve actuator for the chilled water flow rate control. Normally, the actuators are fed by a DC power AC Voltage/power depending on the product specifications. Since different products from various manufacturers have been integrated together as one system in this project, the necessary interface configurations were written into the control software during the commissioning process as per the individual product specifications as shown in Table 2.1

The proportional modulating damper and valve actuators are selected in this control system. Both actuators are fed by a 24 V AC power with a proportional control from 0 to $90°$ opening. The direction of rotation is reversible for both actuators.

Sensor/Actuator	Symbol	Signal range
Temperature	T	20K ohm NTC
Humidity/Temperature senor	R/T	Humidity:4-20mA Temperature: 20K ohm NTC
Differential pressure flow meter	P	0-10Volt
Water flow meter	m	4-20mA
Damper motor	DM	2-10VDC

Valve motor	VM	2-10VDC	
solid-state silicon rectifiers (Heater)	SSR	2-10VDC	

Table 2.1 Input and output configuration

2.3.4 Control Points I/O Board Configuration

Table 2.2 summarizes the sensor descriptions, measured variables, units and the I/O board terminal locations connected to the controllers.

Variable measured	Symbol	Unit	I/O board terminal
Air inlet temperature	T_{a_in}	℃	UI1
Cold duct temperature	Ta_c	℃	UI2
Mixed air temperature	Ta_m	℃	UI3
Hot duct temperature	Ta_h	℃	UI4
Chilled water supply temperature	$Tchws$	℃	UI5
Chilled water return temperature	$Tchwr$	℃	UI6
Mixed air flowmeter	Pm	in WG	SYLK-UI1
Cold duct flowmeter	Pc	in WG	SYLK-UI2
Hot duct flowmeter	Ph	in WG	SYLK-UI3
Chilled water mass flow rate	m_chw	gpm	SYLK-UI4
Cold duct Relative humidity	RHc	%	SYLK-UI5
Inlet Relative humidity	RH_{in}	%	SYLK-UI6
Inlet heater	U_{h_in}	%	AO1
Three-way valve	U_{valve}	%	AO2
Hot duct damper	U_{d_h}	%	AO3
Hot duct heater	U_{h_h}	%	SYLK-AO1
Cold duct damper	U_{d_c}	%	SYLK-AO2

Table 2.2 Sensor description and legends

CHAPTER 3   OPEN LOOP RESPONSES OF THE DUAL-DUCT SYSTEM

3.1 Introduction

A better understanding of the open loop dynamic responses of the system subject to step changes in input variables is important in establishing a good operating range for the system. This information will be quite useful in the design of controllers and as well as control strategies for the system. With this as the motivation, experiments were conducted to study the open loop responses of the dual duct system under different control variables. From the open loop test results, the system's mechanical and thermal dynamic performance (such as operational range, and actuator effective operational range) will be established. In this chapter, the following sub-systems will be evaluated in terms of dynamic and steady-state performances.

1. Airflow sub-system consisting of air flow in the hot and cold air ducts
2. Water flow sub-system
3. Discharge air temperature sub-system

3.2 Airflow Sub-System

The experimental results in this section present the dynamic and steady state performance of the airflow sub-system in each duct (cold and hot) as well as the airflow interactions between the positions of these two dampers. In order to eliminate the effects of other variables on the system, only the air system is activated. Therefore, the variables for the airflow rate are the fan speed and the damper position in the respective ducts.

3.2.1 Steady-State Characteristics

Figures 3.1 and 3.2 show the supply airflow rate under different fan speeds and damper positions. In these experiments, both duct airflow rates are independent from one another in order to get the airflow rate operational range under the stable minimum and maximum fan speed (500 RPM to 1500 RPM). In other words, the cold duct experiments were performed by varying the cold duct damper position and keeping the hot duct damper fully closed, and vice versa for the hot duct experiments. The results show that the maximum supply airflow rate to the cold duct is 176 CFM lower than that of the hot duct air flow rate under the maximum fan speed. However, this is reasonable since the flow resistance in the cold duct is higher than the flow resistance in the hot duct, which is caused by the complex geometry of the cooling coil as opposed to the heating coil. Moreover, the most important thing to note from the figures is that the airflow rate is a linear function of the damper position in both ducts. Also, from a control point of view, the most effective range of operation is 20% to 80% open position for the dampers.
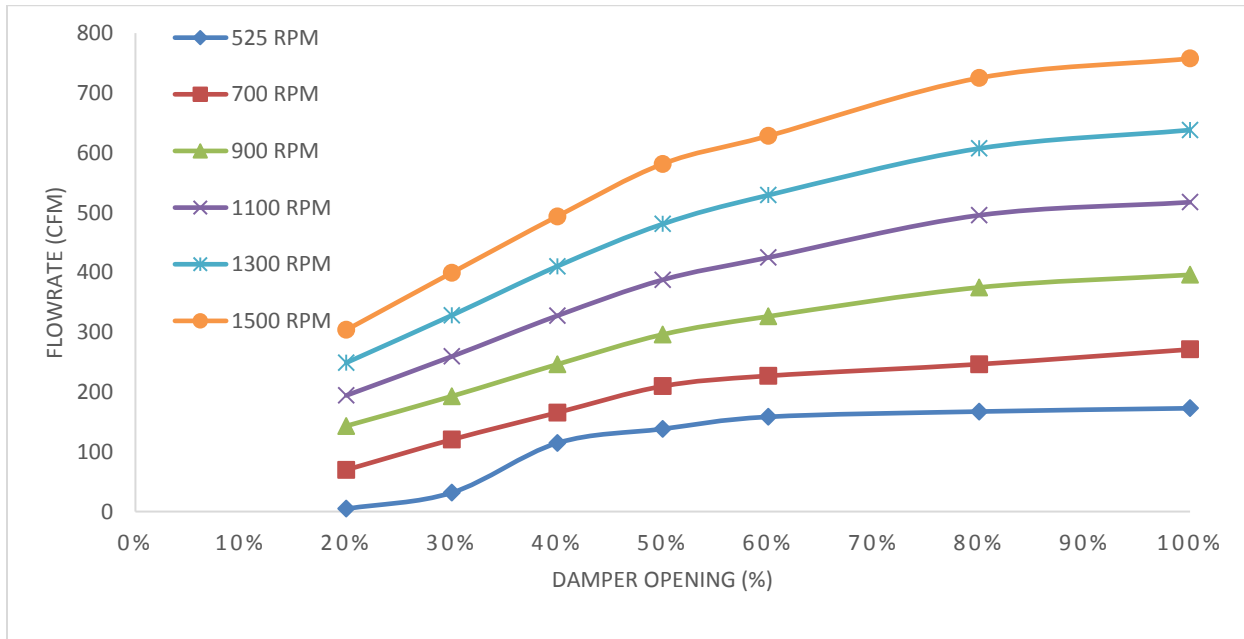
Figure 3.1 Airflow rate under different fan speed and damper positions in cold duct
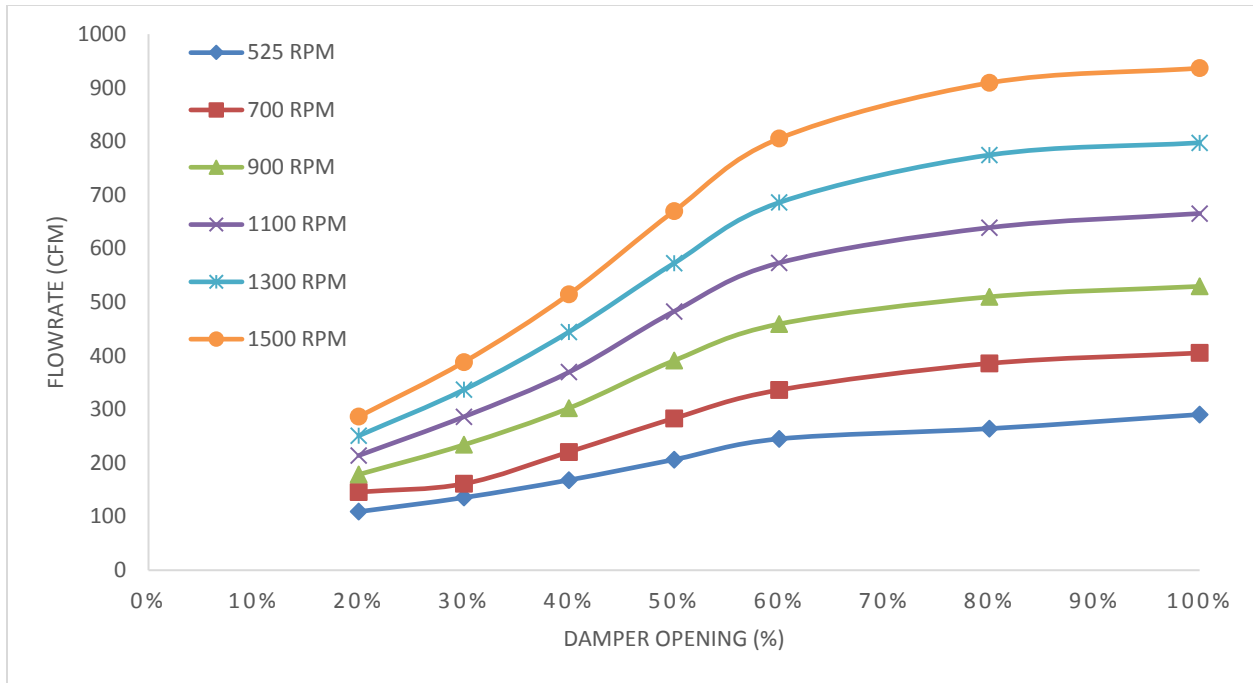
Figure 3.2 Airflow rate under different fan speed and damper positions in hot duct

To determine the airflow rate balance in the entire system, experiments were conducted at a fixed fan speed (1100RPM). The hot duct damper position was varied while holding the cold duct damper in the fully open position. The results are depicted in Table 3.1. The sum of the airflow rates from both ducts should equal the airflow rate in the mixed air duct. The rate of error is calculated based on the sum of airflow rates in both ducts with respect to the measured airflow rate in the mixed air duct. As may be noted from the table, there is a 7.6% error when both dampers are fully open and an 11.1% error when the hot duct damper was set at 25% open position. This discrepancy is caused by the inaccuracy of the flow sensors as well as the resistance to airflow in the duct system. Also of note is the fact that the supply airflow rate is about 250 cfm lower than the hot duct airflow rate when both dampers are in the fully open position.

Hot damper open	Cold duct (cfm)	Hot duct (cfm)	Mixed air duct (cfm)	% error
100%	199.39	447.16	699.69	7.6
75%	226.09	404.40	688.49	8.4
50%	321.86	271.50	648.62	8.5
25%	416.27	110.67	592.48	11.1

Table 3.1 Airflow repartition in the system

3.2.2 The effects of damper position on the duct air flow rates

Since the experimental facility is built as a single fan dual duct system, one important question in the operation of the system is the airflow interactions within the two ducts. To study and qualify the effects in terms of changes in air flow rate, several experiments have been conducted by holding one damper position constant and changing the other. The results are plotted in Figures 3.3 to 3.6.

These figures show the effects regarding changes in airflow rate in both ducts by changing the hot duct damper position while holding the cold duct damper at a fully open position as well as holding the fan speed constant at 1100 RPM. The curves in Figure 3.3-3.6 show that the damper position impacts the airflow rates nonlinearly. Also, at wide open damper positions (75% and 100%), the air flow in the hot duct is much higher than in the cold duct. On the other hand, when both dampers are narrowly opened (50% and 25%), the air flow is mostly the same in the ducts. This phenomenon could also be explained by the discussion of flow resistance in both ducts in section 3.2.1. Moreover, a zero flow rate may occur at 25% opening of the cold duct damper. From a control point of view, to control the mixed air temperature via damper position, the hot duct damper is the better choice since it is easier to control and has a larger control range (0-450 CFM).
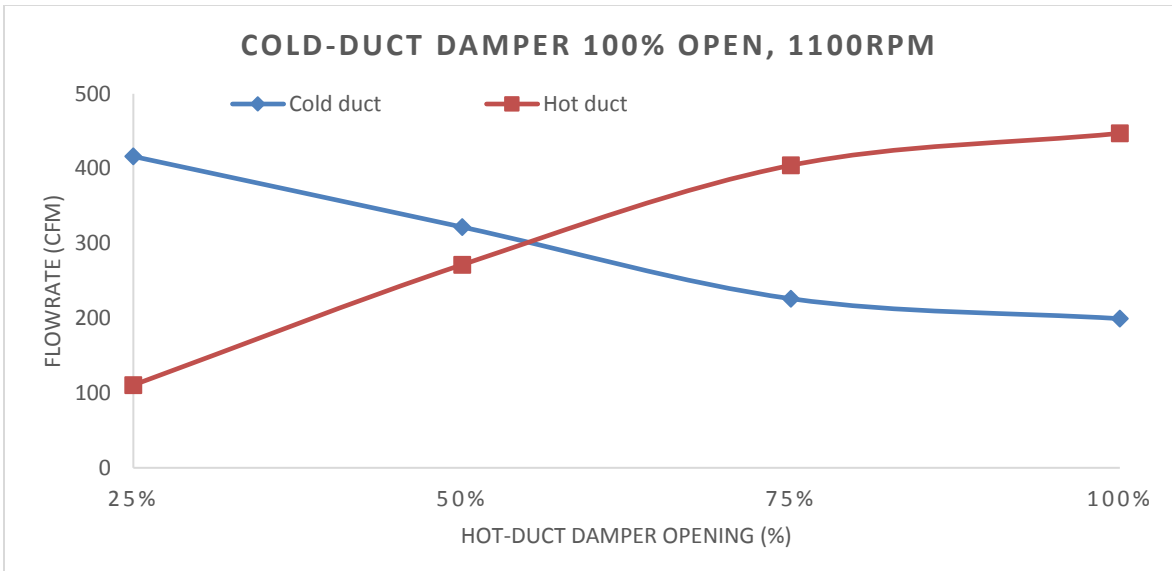
Figure 3.3 Air flow interaction in the dual-duct system
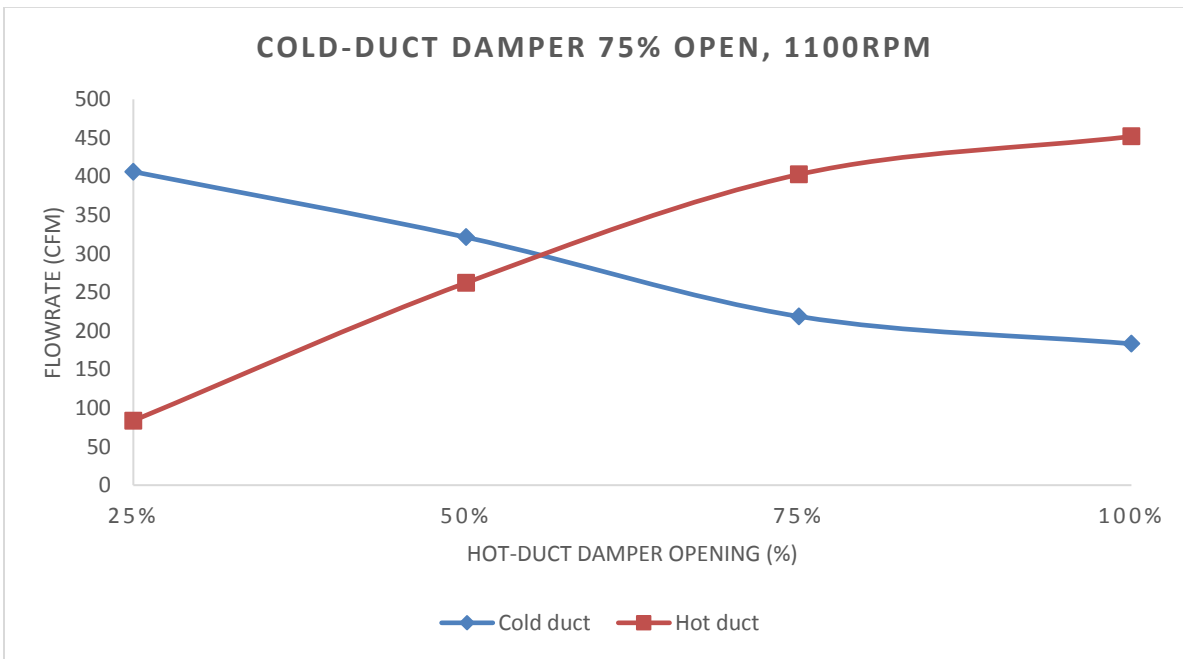
Figure 3.4 Air flow interaction in the dual-duct system
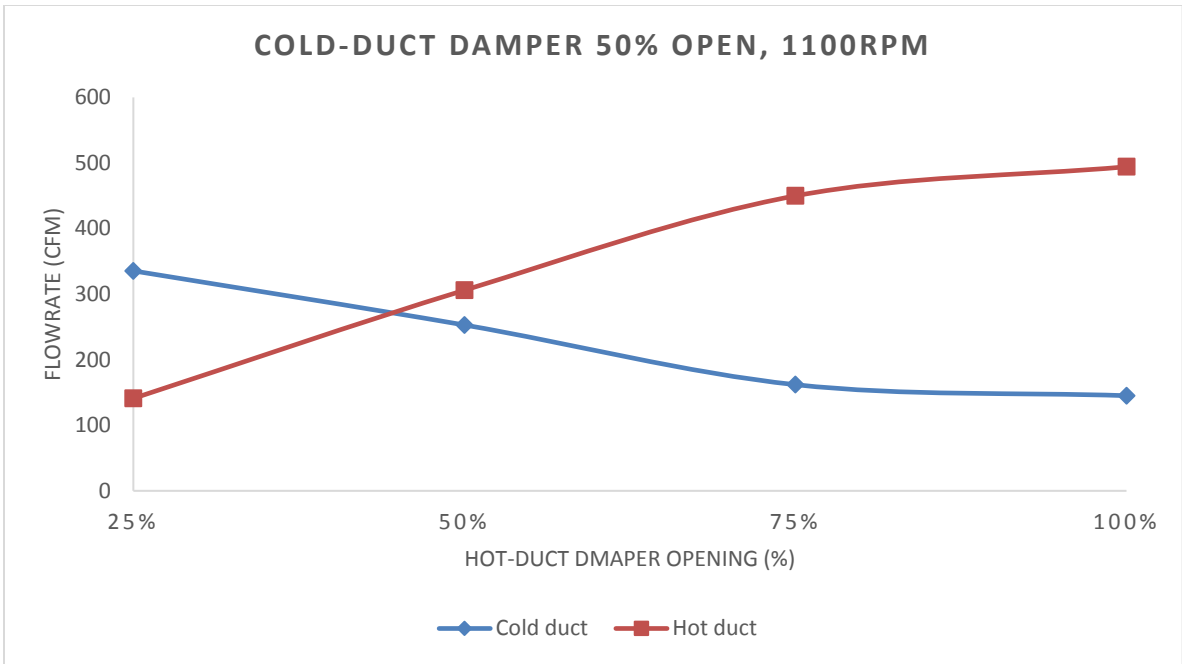
Figure 3.5 Air flow interaction for the dual-duct system
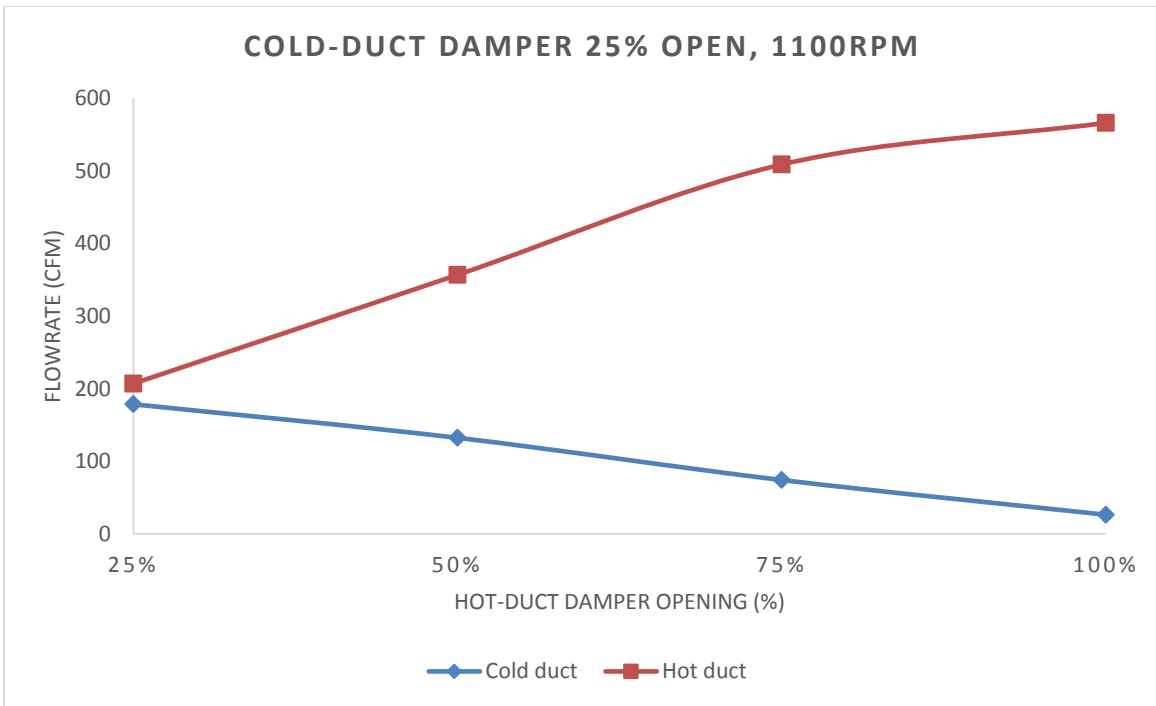
Figure 3.6 Air flow interaction in the dual-duct system

3.2.3 Dynamic responses of the airflow subsystem

To determine the dynamic response of the air flow system when changing the damper position, several experiments were conducted and the results are plotted in figures 3.7 to 3.14. In these figures, the air flow rates in both ducts are functions of time at different damper positions (figure 3.7, 3.9, 3.11, and 3.13). Figure 3.8, 3.10, 3.12 and 3.14 show the time response characteristics of the damper. In other words, these figures depict the time required for the air distribution system to reach a steady state as well as the dead-time, which is the time needed for the control signal to reach the actuator causing a measurable output to appear. As shown in Figure 3.7, it takes between 160s -180s for the system to reach a stable state when the damper opens from the fully closed to the fully open position. Likewise, the system steady state times of 140 seconds, 100 seconds and 70 seconds were recorded corresponding to the 75%, 50% and 25% open damper positions, respectively. Furthermore, as shown in Figures 3.8, 3.10, 3.12, and 3.14, the damper position starts to change 30 seconds after the control signal input is given. Therefore, the dead-time of the air distribution system is 30 seconds.
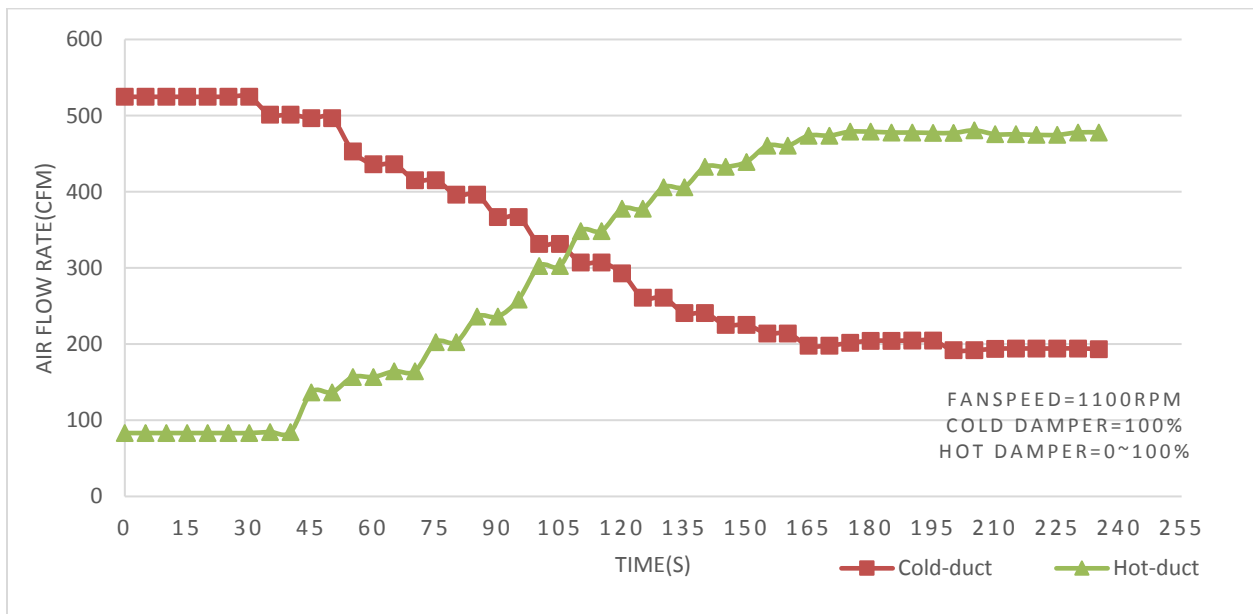
Figure 3.7 Dynamic responses of airflow sub-system under different damper openings

35
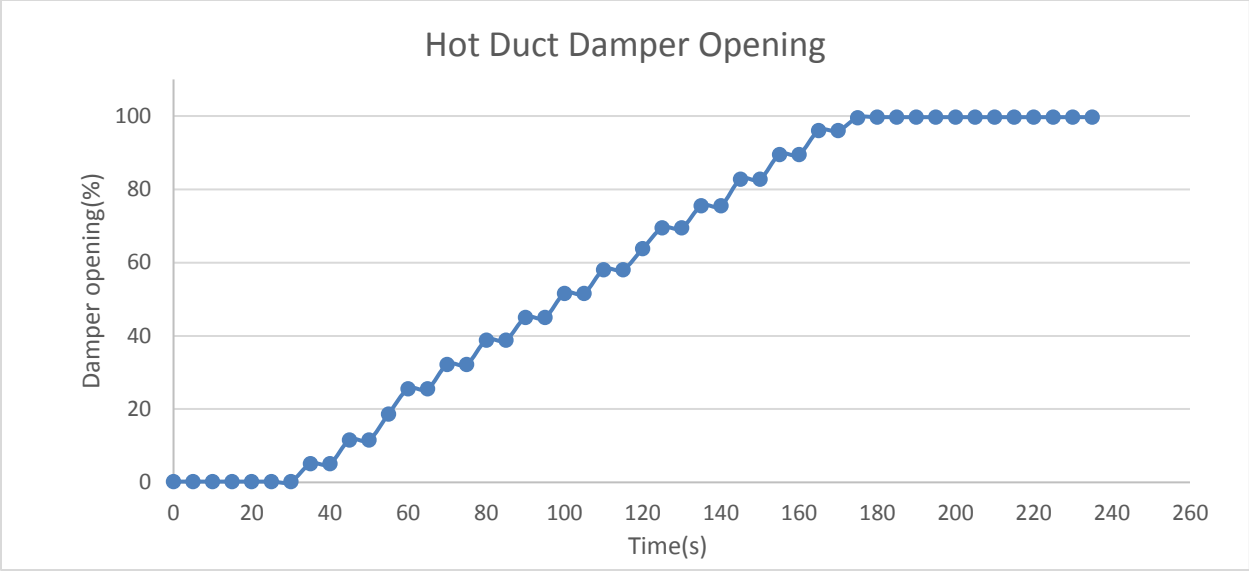
Figure 3.8 Dynamic responses of damper position under different damper openings
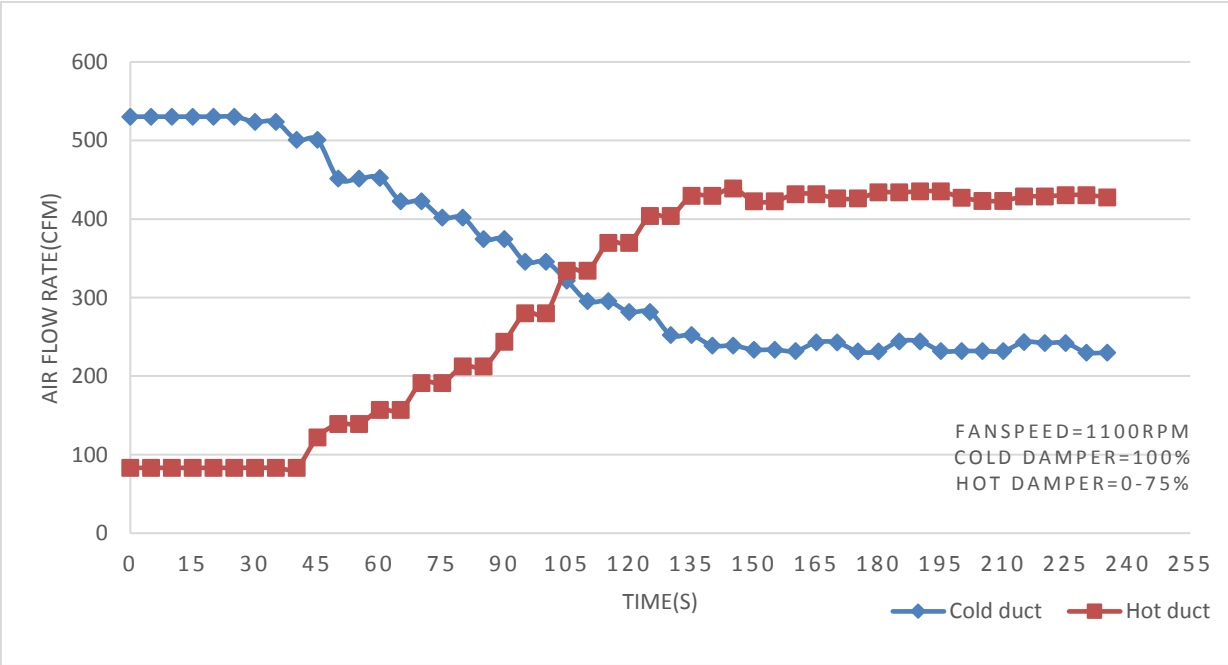
Figure 3.9 Dynamic responses of airflow sub-system under different damper openings

36
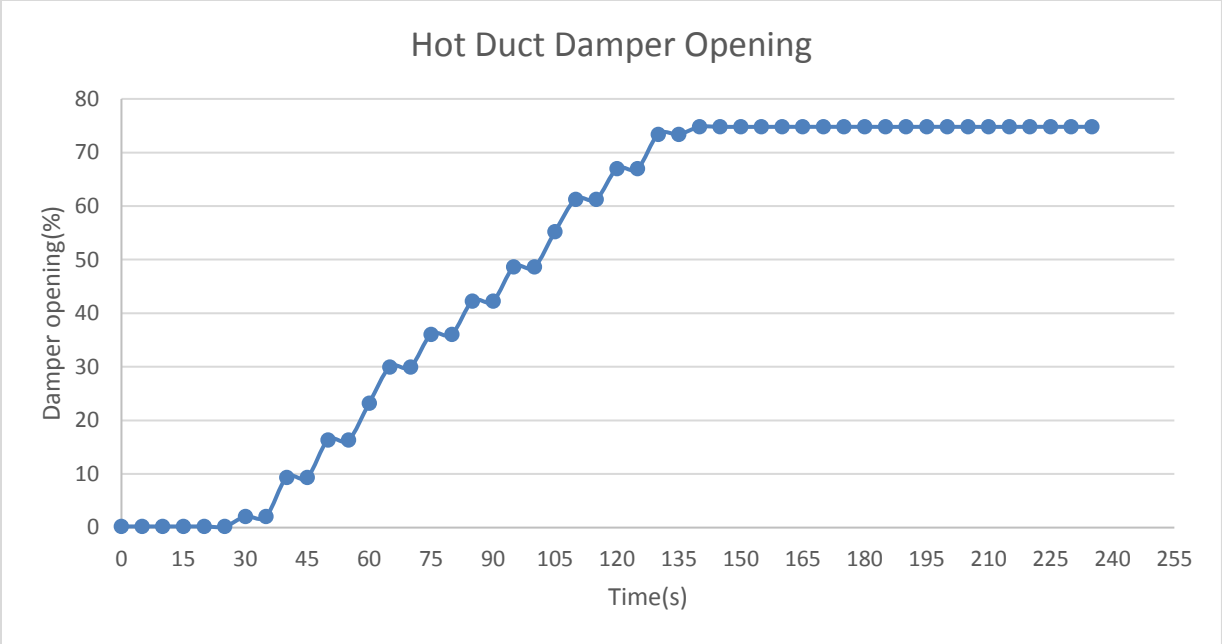
Figure 3.10 Dynamic responses of damper position under different damper openings
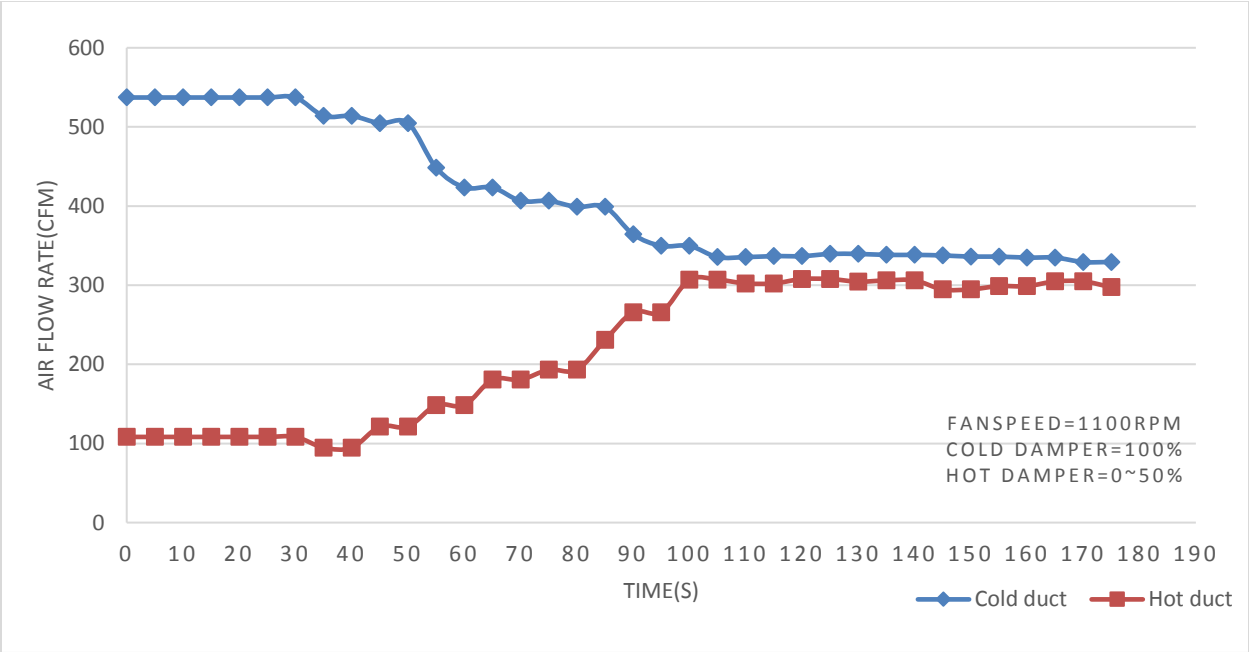
Figure 3.11 Dynamic responses of airflow sub-system under different damper openings
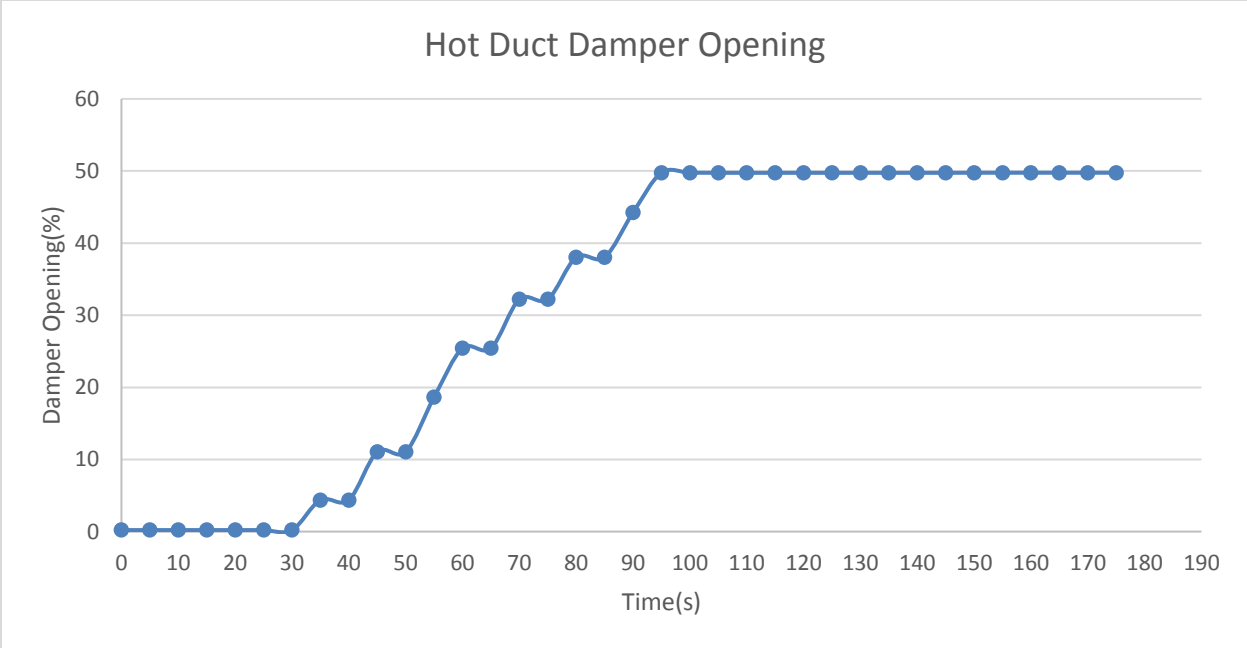
Figure 3.12 Dynamic responses of damper position under different damper openings
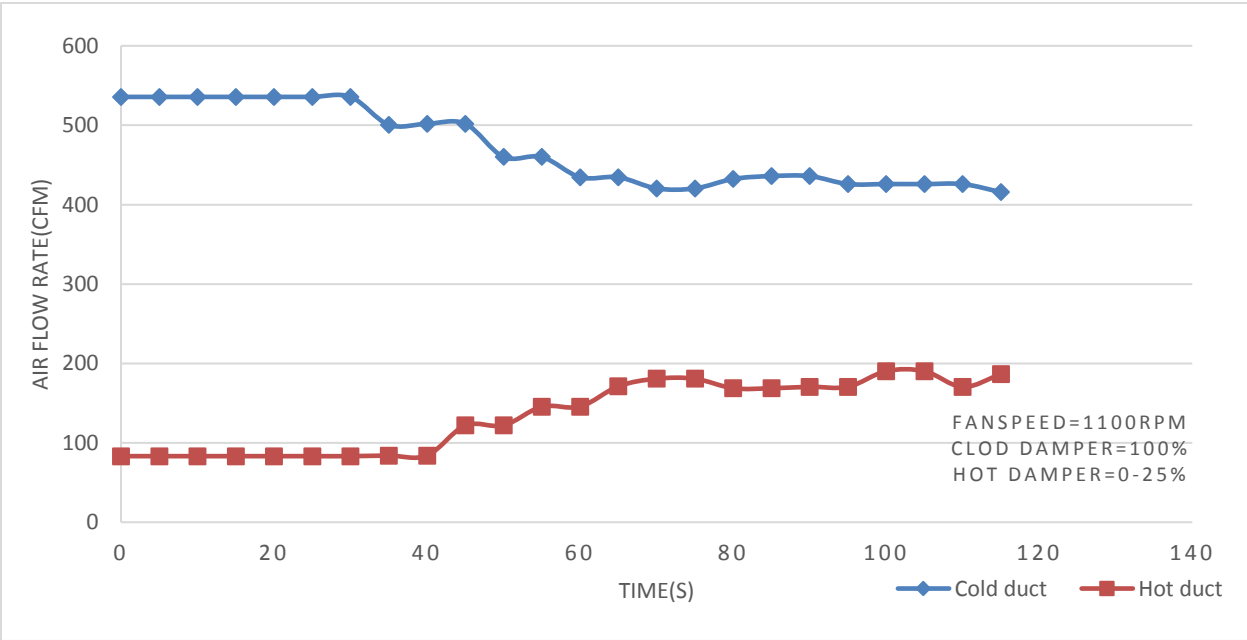
Figure 3.13 Dynamic responses of airflow sub-system under different damper openings
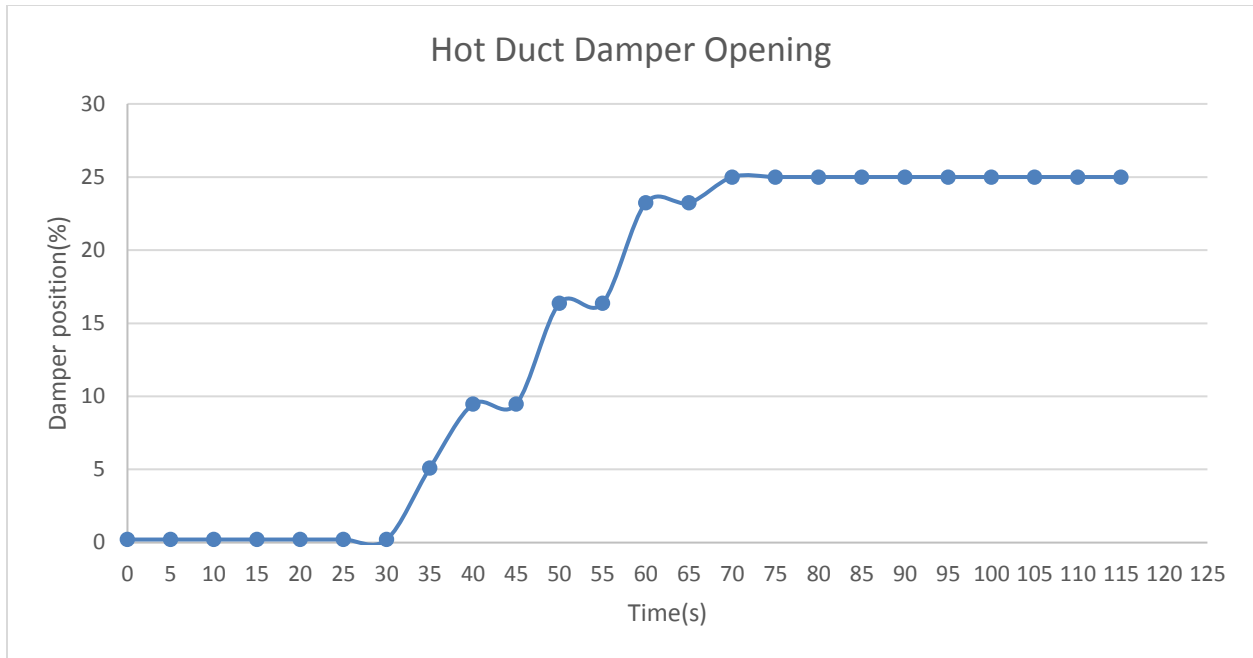
Figure 3.14 Dynamic responses of damper position under different damper openings

These figures are very useful in establishing the proper range of operation of the system and the dead time characteristics of the actuators.

3.3 Water flow sub-system

The dynamic responses of the discharge air temperature system are influenced by the water flow sub-system, which is affected by the three-way valve characteristics. The experimental results in this section show the steady and dynamic relations between the water flow rate as a function of the three-way valve position.

3.3.1 Steady-state characteristics

Since the water flow rate is influenced by the three-way valve position, several experiments were

conducted to determine the characteristics of the three-way valve. Figure 3.15 shows that the maximum water flow rate is 6 GPM and the operational range of the valve is between the 36% and 100% open positions. Furthermore, the curve shows a linear relationship between the water flow rate and the valve position, which is good for the control design.
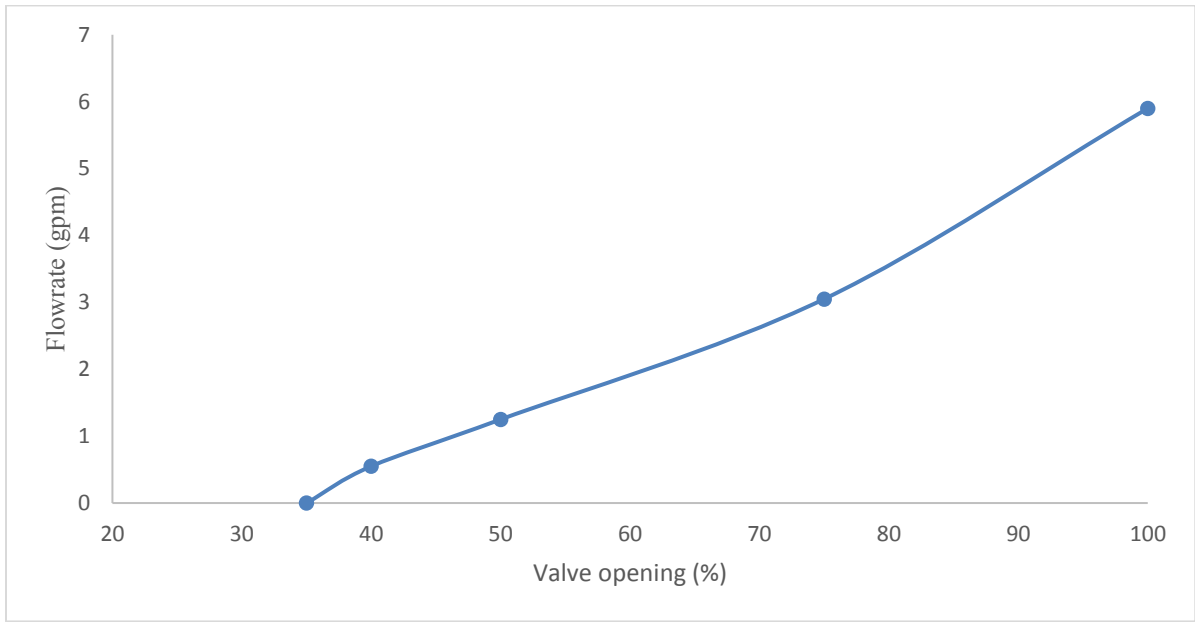
Figure 3.15 Water flow rate as a function of valve position

3.2.2 Dynamic response of the water flow sub-system

As we can see from Figure 3.16, the water flow rate changes as the three-way valve position changes from the 100% to the 75% open position. The control range of the valve was found to be between 36% open and 100% open. Figure 3.16 shows that the water flow system needs around 60 seconds to reach the stable state. A 30 second dead time was also observed in the valve actuator response.
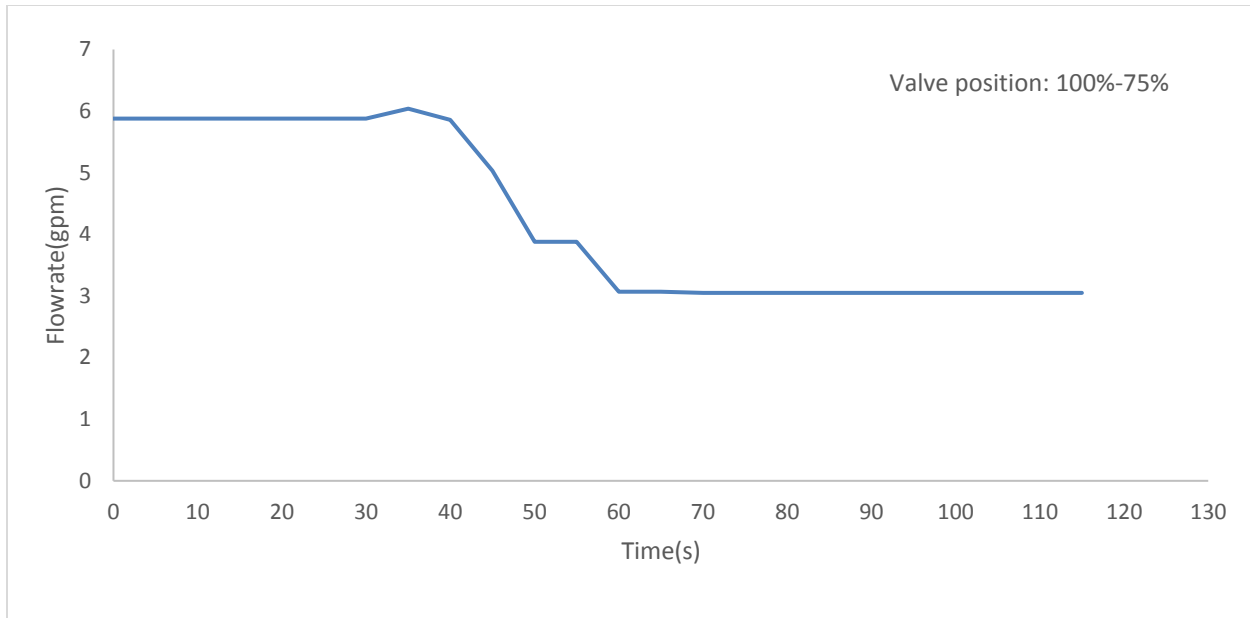
Figure 3.16 Dynamic response of water distribution due to a step change in the valve position

3.4 Discharge air system dynamic response

The discharge air system is one of the most basic components in heating, ventilation, and air-conditioning systems (HVAC). To determine the dynamic performance of the discharge air system (DAS), several experiments have been conducted and the results are plotted in figures 3.17 to 3.20. In this case, the fan speed, valve position, water flow rate, chilled water supply temperature (CHWST) and chilled water return temperature (CHWRT) constitute the input to the discharge air system. The output is the discharge air temperature (DAT). Note that all the experiments are conducted with a fully open cold duct damper and a fully closed hot duct damper. The chiller system works with its built-in controller. The chilled water is supplied to the cooling coil at an average temperature of 7℃. The maximum and minimum water temperatures from the chiller were respectively, 7.7℃ and 5.7℃.

Figure 3.17 depicts the dynamic responses of the discharge air system under full load with a fan speed of 1500 RPM when the valve opens from 0 to 100%. The discharge air temperature

41

reaches the steady state value of 14°C in about 600s. The chilled water supply temperature is fluctuating between 7.7°C and 5.7°C. Likewise, the water return temperature is also fluctuating between 9.6°C and 8.1°C. Note that the maximum water flow rate when the valve is 100% open is about 6 gpm and it reaches a steady state within 100 seconds. Again, the dead-time for the discharge air system is around 30 seconds.
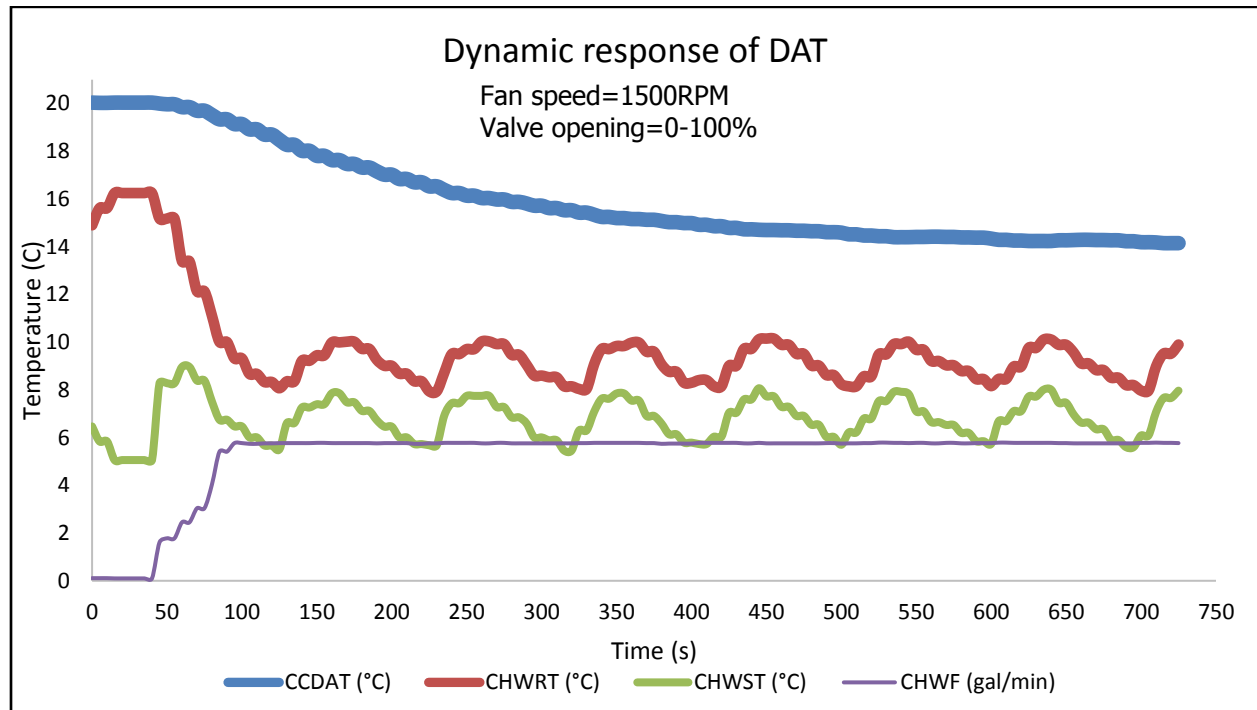
Figure 3.17 Dynamic responses of DATS

To study the dynamic performance of the discharge air temperature under different fan speeds and three-way valve positions, several experiments have been conducted. One concern regarding the experimental conditions is the initial condition of the air temperature should be the same since the initial condition does have an effect on the steady state time. We should also note that the zone environment has some effect on the inlet air temperature as well, since the experimental facility is installed indoors in the lab and the cooled air is also vented in the lab.

Figures 3.18-20 depict the discharge air temperature dynamic responses with different valve positions at constant fan speed (load). The results show that the processes require the same

amount of time, which is around 600 seconds, to reach a steady state under different fan speeds and valve openings. Also, under full load conditions (1500 RPM) and at a valve position of 40% and a chilled water temperature of 7 degrees (average), the discharge air temperature increases to 17.5 degrees. On the other hand, the discharge air temperature can decrease to as low as 11 degrees when the fan speed is reduced to 500 RPM.
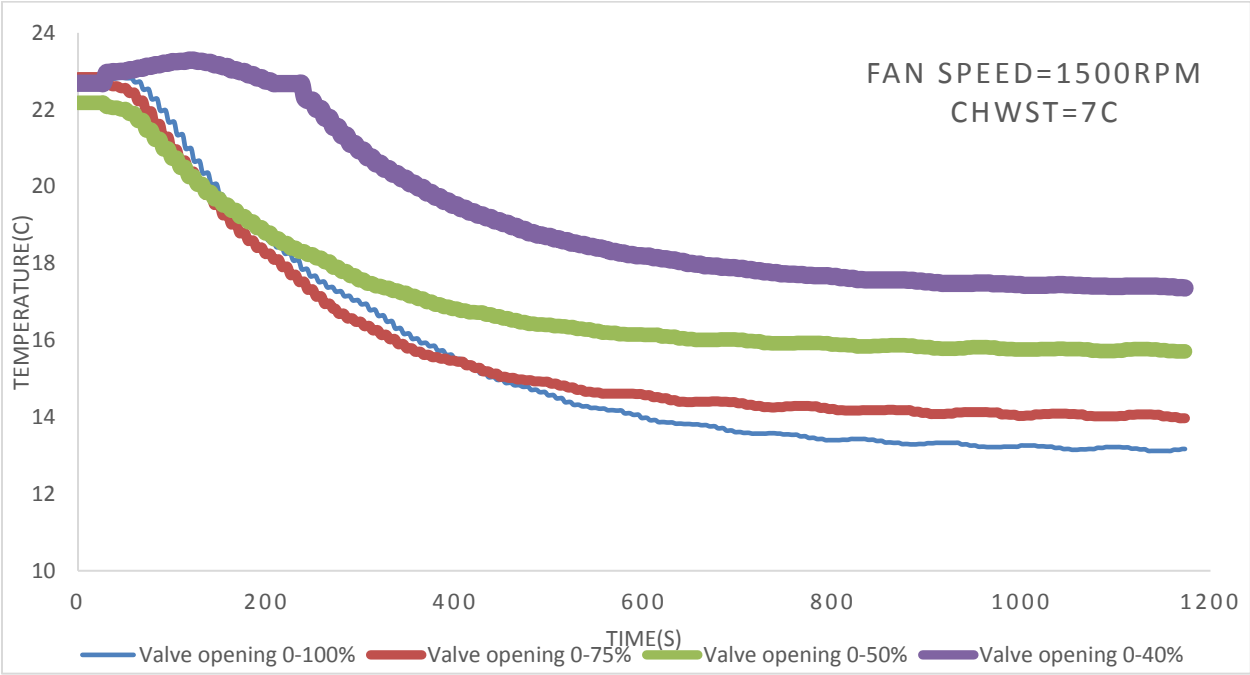
Figure 3.18 DAT response at different valve positions with a constant fan speed

43
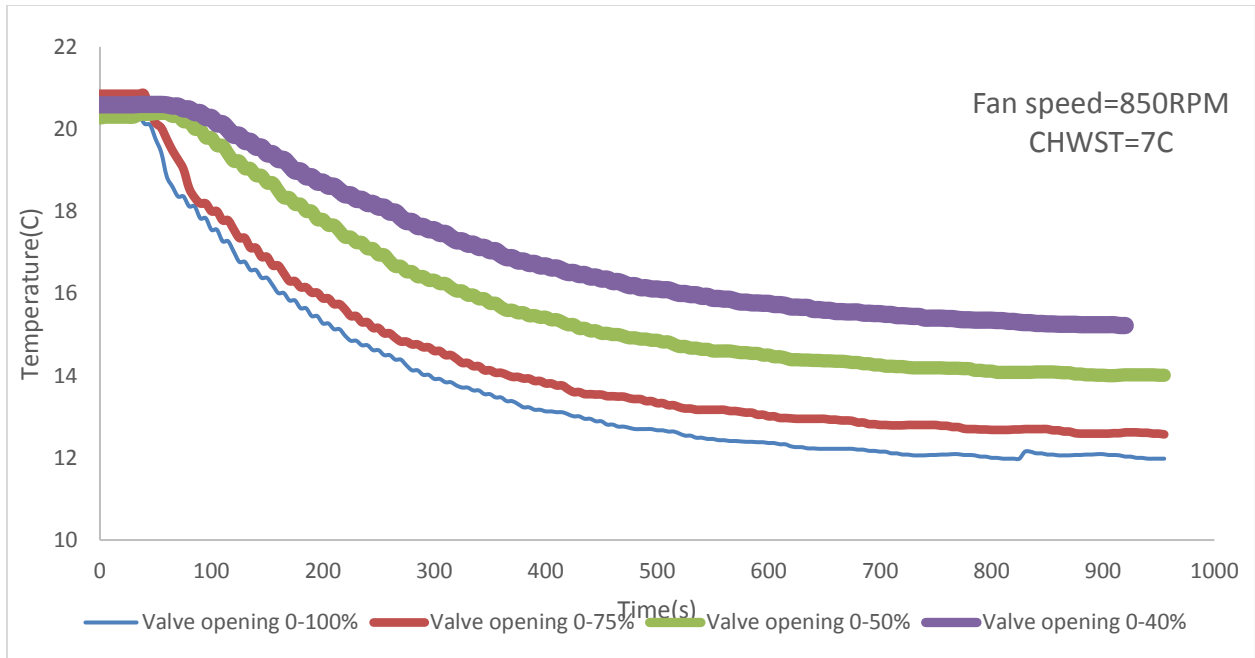
Figure 3.19 DAT response at different valve positions with a constant fan speed
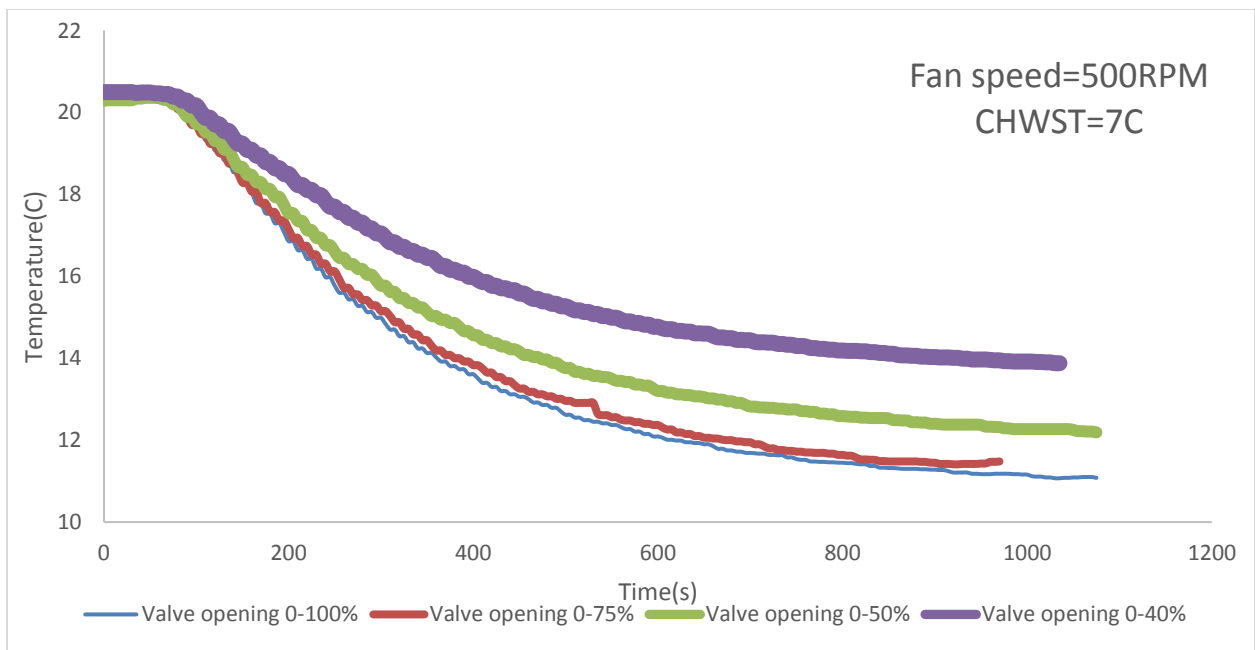
Figure 3.20 DAT response at different valve positions with a constant fan speed

3.5 Summary and conclusions

In this chapter, a series of open loop tests were conducted to identify the steady state characteristics and dynamic performance of the following three sub-systems: (i) the air flow sub-system, (ii) the water flow sub-system and (iii) the discharge air system. From the open loop test results, the systems' mechanical and thermal dynamic performance, such as operational range, and actuator effective operational range, were identified. Through the test results, the following conclusions were drawn:

(1) The air flow rate is a nonlinear function of the damper position, and the maximum flow rate in the cold and hot ducts is 757 CFM and 936 CFM respectively.

(2) The steady state times for 100%, 75%, 50% and 25% damper opening are 180 seconds, 140 seconds, 100 seconds and 70 seconds respectively.

(3) Large hot duct damper openings and smaller cold duct damper openings could lead to zero air flow in the cold duct. It is therefore better to control the mixed air temperature through the hot duct damper for this system. This result was the basis for selecting the hot duct damper position to control the mixed air temperature.

(4) The operational range of the chilled water three-way valve is between 40% ~100%. The maximum chilled water flow rate was found to be 6 GPM and the steady state time is 100 seconds.

(5) The discharge air temperature reaches a steady state in about 600s under various load conditions (fan speed), which means the steady state time is not significantly affected by the load.

(6) The controllable discharge air temperature range is between 14°C ~17.5°C under full load conditions and the lowest discharge air temperature obtained was 11°C.

(7) Since the chiller works with its built-in controller, the chilled water supply temperature from the chiller was fluctuating between 7.7°C and 5.7°C while the chilled water set-point was set at 7°C.

(8) The dead time for all the sub-systems was found to be 30 seconds

CHAPTER 4　　Manual Tuning of the Controllers and Gain Scheduling Control

4.1 Introduction

In this chapter, a gain scheduling control for HVAC control loops will be developed. The control performance of the gain scheduling control will be compared with the conventional PI control. To this end, a base case conventional controller will first be designed for the discharge air system control loop. For this purpose, the Ziegler-Nichols tuning rules were applied to determine the PI control gains. The controller output equation is:

$$u(t) = k_p e(t) + k_i \int e(t) dt + u_0 \qquad \text{(eq. 4.1)}$$

Where

k_p and k_i are the proportional and integral gains, respectively.

$e(t)$ is the variable error in the control variable from its set $-$ point.

Depending on the product design, the proportional term could be the proportional gain (kp) and proportional band (PB). The relationship between the proportional gain and proportional band is defined in the Honeywell product manual as:

$$PB = \frac{1}{k_p} \qquad (eq. 4.2)$$

However, from the experiment results, it was found that the tuning parameters determined by the Ziegler-Nichols method could not produce good control performance when a sudden set-point change was imposed. Therefore, a gain scheduling control algorithm has been proposed and its performance will be compared with Ziegler-Nichols method.

46

This chapter will focus on the following topics: (i) dynamic response of the discharge air temperature control loop tuned by the Ziegler-Nichols method, (ii) gain scheduling control of the discharge air temperature control loop and its modification, (iii) a new adaptive control algorithm development and (iv) verification of the performance of the new adaptive control through computer simulations.

4.2 Ziegler-Nichols tuning method

4.2.1 The tuning parameters

To determine the tuning parameters of the control loops based on the Ziegler-Nichols method, the ultimate sensitivity (P) and ultimate period of oscillation (T) must be obtained from several closed loop tests. By setting the derivative and integral actions to zero, the controller proportional band was adjusted until the output responses showed a constant period of ultimate oscillation about the set-point. At this point, the proportional band is the ultimate sensitivity. The set-point was set to 14.5℃. Figure 4.1 shows that as the proportional band decreases, the control loop reaches its constant oscillation about the set-point with PB=0.2 under full load conditions. During the tests, the chilled water supply temperature was kept around 7℃, the fan speed was held constant at 1500 RPM, the cold duct damper was fully opened and the hot duct damper was fully closed. From the figure, the ultimate sensitivity (P) is equal to 0.2 and the period of ultimate oscillation (T) is equal to 180s. Therefore, according to the Ziegler-Nichols tuning method for PI control, the proportional band and the integral time were established as:

$PB = 2.2P = 0.44$

$T_i = 0.8T = 144\ seconds$

Experiments were conducted with these PI controller gains and the discharge air temperature responses under different operating conditions were studied.
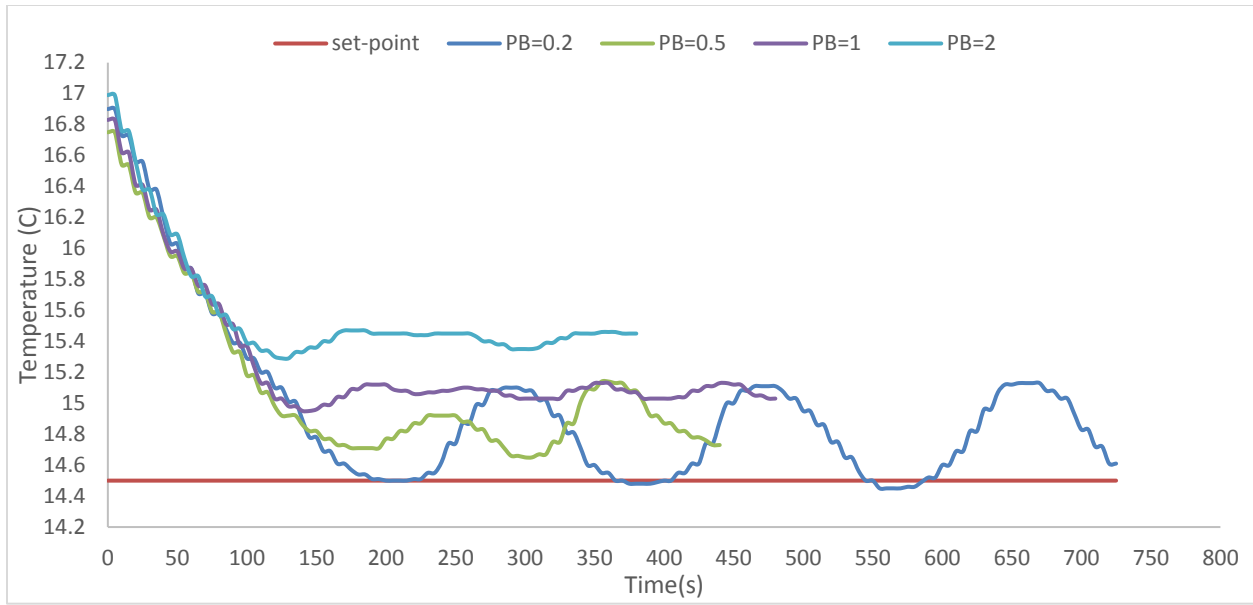
Figure 4.1 Closed-loop test on discharge air temperature loop

4.2.2 Dynamic responses of DAT loop

Figure 4.2 shows the dynamic response of the DAT loop, which is controlled by modulating the three valve position under the full load conditions as described in section 4.2.1. The DAT reaches its set-point from the initial condition of 21.3℃ in about 400 seconds with no undershoot. Furthermore, there is only a small oscillation of ±0.1℃. In other words, the control is very fast, stable and smooth.

However, with the parameter determined by the Ziegler-Nichols method, the control loop gives a fast but unstable response when a set-point change of 2℃ is applied (from 14.5℃ to 16.5℃) as indicated in Figure 4.3. The responses show that the three-way valve executes the action immediately when the set-point change has been applied and reaches steady state in about 200 seconds with an oscillation of +1℃ and −0.5℃.

To eliminate the oscillation due to set-point change, the proportional band was increased to 1.1 and the integral time was kept the same (144s). The result is plotted in Figure 4.4. The DAT takes longer (500 seconds) to reach its set-point (14.5℃) and it took 800 seconds to re-stabilize

48

after a set-point change of 2°C (from 14.5°C to 16.5°C) was applied.

By comparing the above results, the following observations can be made:

1. The control loop with the control parameters determined by the Ziegler-Nichols method gave poor dynamic performance due to the set-point changes.
2. Increasing the proportional band increased the steady state time. The increase in steady state time was much higher when a set-point change was applied to the system.

To improve the dynamic performance of the control loop, a gain scheduling control will be presented in the following section.
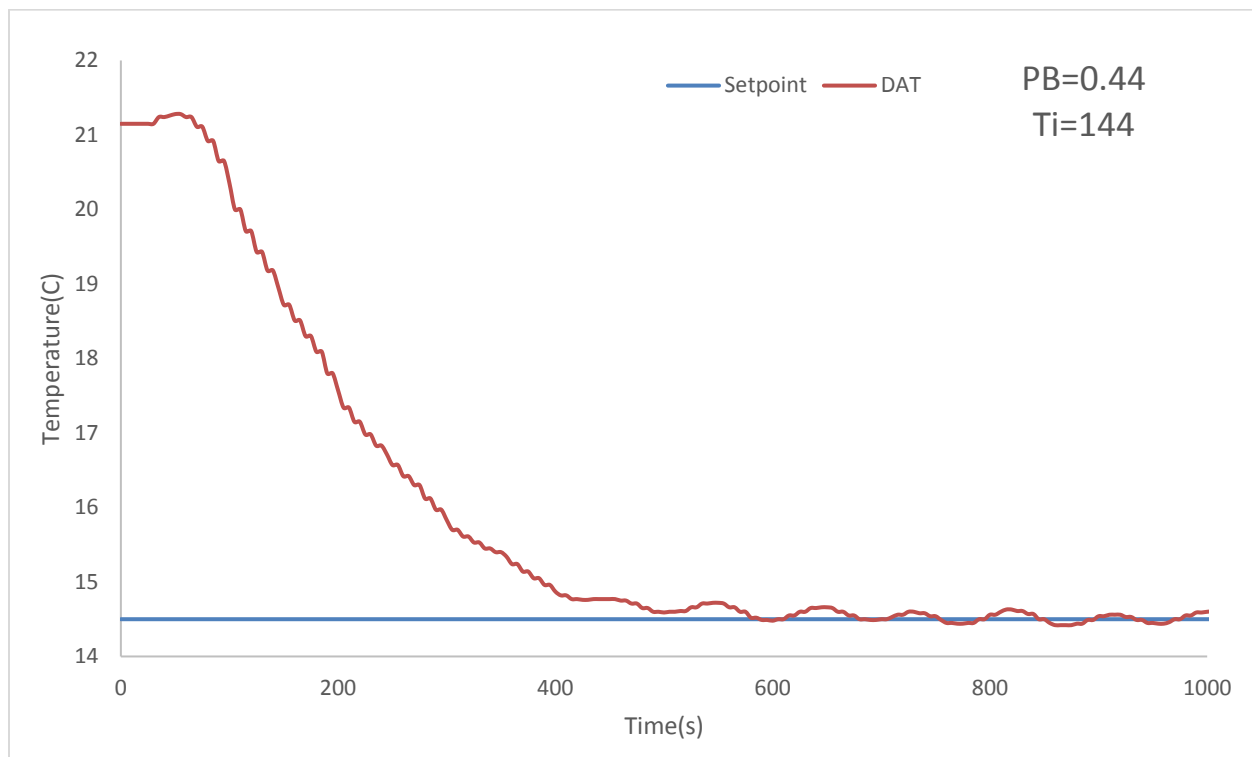
Figure 4.2 PI control of DAT loop (Ziegler-Nichols tuning method)
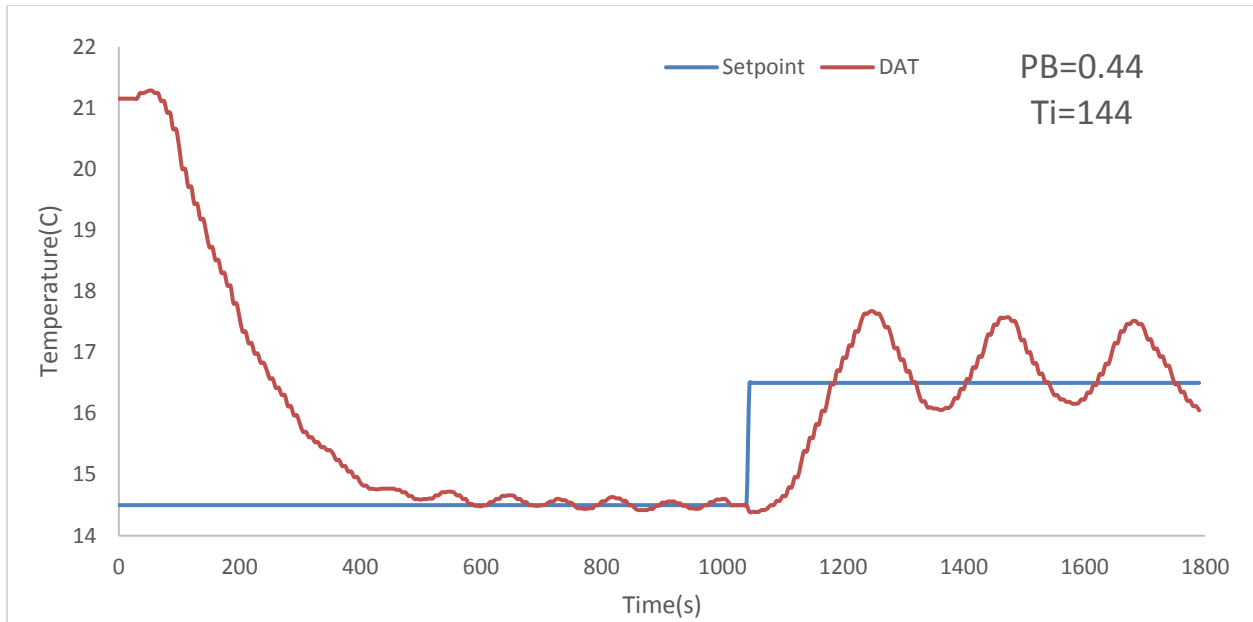
Figure 4.3 PI control of DAT loop due to set-point change (Ziegler-Nichols tuning method)
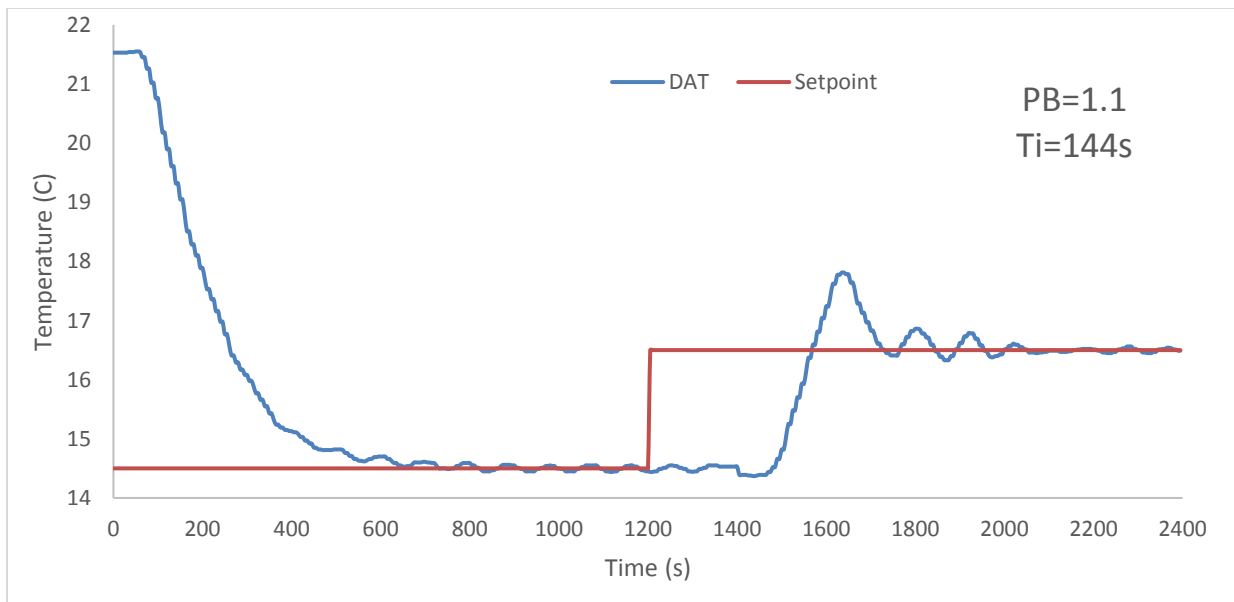
Figure 4.4 PI control of DAT loop due to set-point change (Ziegler-Nichols tuning method)

4.3 Gain scheduling control

Unlike the conventional constant PI control, the concept of gain scheduling control involves changing the proportional gain and integral time according to the error between the control variable and its set-point. In this thesis, Sedaghati's [22] gain scheduling control method has been applied to control the DAT system. In the gain scheduling control, the controller output is expressed by:

$$u(t) = k_p(t)e(t) + k_i(t) \int e(t)dt + u_0 \qquad \text{(eq. 4.3)}$$

where $k_p(t)$ and $k_i(t)$ are functions of the error between the control variables and their set-point e(t) which could be expressed as:

$$k_p(t) = k_p(max) - (k_p(max) - kp(min))e^{-k_1 e(t)} \qquad \text{(eq. 4.4)}$$

$$k_i(t) = k_i(max)(1 - tanh (k_2|e(t)|)) \qquad \text{(eq. 4.5)}$$

where $k_p(max)$ and $k_p(min)$ are the maximum and minimum values of the proportional gains, $k_i(max)$ is the maximum integral time of the control loop (in this case equal to 144 seconds), e(t) is the error between the control variable and its set-point and k_1 and k_2 are the process coefficients determined by the control loop responses. As can be seen from equation 4.4, with a large error, the exponential term will decrease to zero; as a result, the proportional gain will reach its maximum value, leading to a faster response. As the error decreases, the exponential term will approach 1; therefore, the proportional gain will reach its minimum value and give a slow and stable response. For the integral term, when the error is large, the hyperbolic term will become 1. A zero integral time will be expected to accelerate the settling time and when the error is small, a large integral time will be needed to eliminate the oscillations as the hyperbolic term approaches zero. By introducing the PB, the gain scheduling (GS) control equations are rewritten as

$$PB(t) = PB(max) - (PB(max) - PB(min))tanh (k_1|e(t)|) \qquad \text{(eq. 4.6)}$$

51

$$k_i(t) = k_i(max)(1 - tanh\ (k_2|e(t)|))$$
(eq. 4.5)

where PBmax and PBmin are the maximum and minimum values of the proportional band due to the control range of the set-point (in this case, these were $16.5°C\ and\ 14.5°C$ respectively). Experiments were conducted to study the temperature responses of the system with GS control. The results are plotted in Figure 4.5. From the figure, it can be noted that the responses with GS control reached the original set-point in about 400 seconds without undershoot, which matches the performance of the Ziegler-Nichols control method. A small change in the setpoint from a lower to a higher value ($14.5°C\ and\ 16.5°C$) resulted in an overshoot of $1.2°C$ and the set-point was reached in about 300 seconds. Furthermore, decreasing the setpoint from a higher to a lower value resulted in a better response with a settling time of 200 seconds and no undershoot. A comparison with the Ziegler-Nichols control responses shows that the responses from the GS control have the same settling time; however, the steady state time was much lower (from 800 seconds to 300 seconds) due to a change in set-point, and the overshoot was reduced from $1.3°C$ to $1.2°C$.
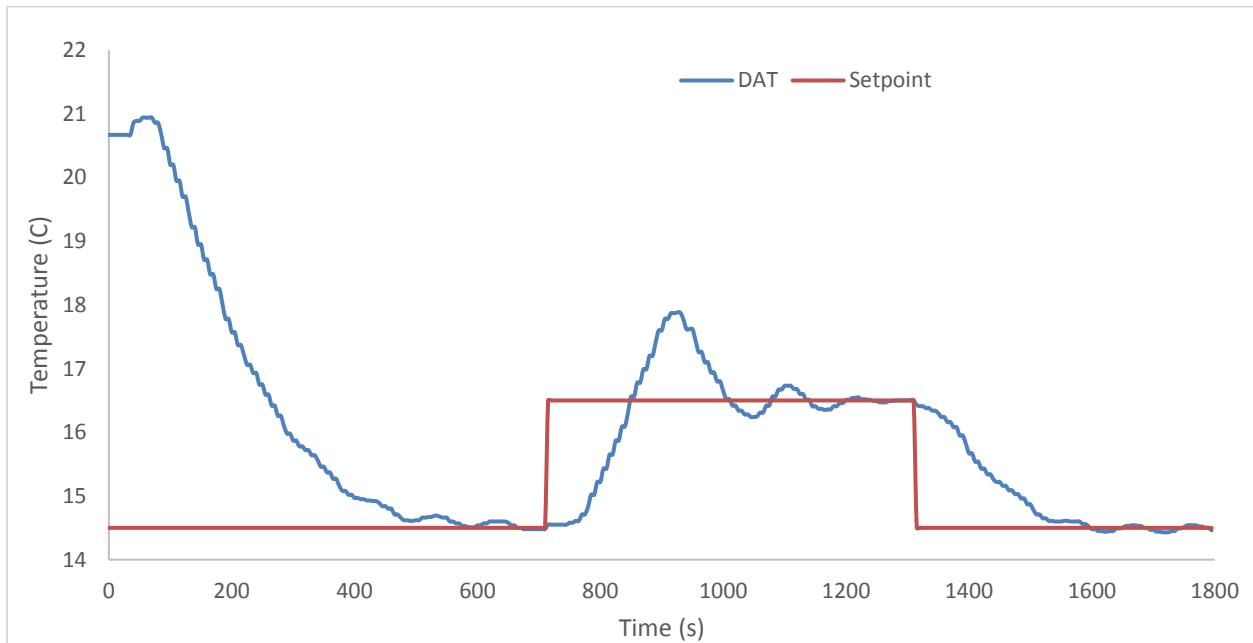
Figure 4.5 Gain scheduling PI control of DAT loop due to set-point change

The parameters used in the experiments are shown in Table 4.1.

Parameter	PB(max)	PB(min)	$k_i(max)$	k_1	k_2
Value	1.76	0.44	144s	1	1

Table 4.1 Control parameters for modified gain scheduling control

4.4 Adaptive Gain Scheduling Control Method

4.4.1 Adaptive Gain Scheduling Control

Although the gain scheduling control provides a good control due to the set point changes, the process of finding the five control parameters by trial-and-error is still very time-consuming. These parameters also need to be modified for different load conditions. As the proportional band becomes smaller, the responses oscillate for the case in which the setpoint was increased from a lower to a higher value (low load case). In contrast, as the proportional band becomes larger, the responses showed higher overshoot and longer settling times for high load conditions. Also, it was found that the gain scheduling control method caused significant oscillations and took nearly 25 minutes to reach a stable final value for the low load condition (Figure 4.8). To address these limitations, an adaptive gain scheduling control is proposed. The proposed adaptive control is based on the thermal dynamics of the chilled water and discharge air control loops.

From a control point of view, the PI control initially requires a small proportional band (PB) when a sudden set-point change occurs due to load disturbance. However, as the control variable approaches its set-point, a large proportional band is required to stabilize the output. To this end, an adaptive control parameter which captures the load dynamics and updates the PB was added to the gain scheduling control equation. The adaptive parameter was defined as a ratio ($\frac{|e(t)|}{\Delta T_{chw}}$) which captures the dynamics of the discharge air temperature and the chilled water system interactions. From the experimental results, it was noted that the chilled water temperature difference increases as the discharge air temperature set point increases, as shown in Figure 4.6.

However, since the chilled water temperature is on-off controlled, the use of this adaptive parameter in the control induces cyclical disturbance in the system. For this reason, the adaptive parameter was modified as $\frac{|e(t)|}{\Delta T_{chw,max}}$. By using this adaptive parameter, an adaptive gain scheduling (AGS) control is proposed in which the PB is continuously updated by the following equation:

$$PB(t) = PB(max) - (PB(max) - PB(min)\ )tanh\ (\frac{|e(t)|}{\Delta T_{chw,max}}|e(t)|) \qquad \text{(eq. 4.7)}$$

$$k_i(t) = k_i(max)(1 - tanh\ (k_2|e(t)|)) \qquad \text{(eq. 4.5)}$$

where PBmax and PBmin are the maximum and minimum values of the proportional band. As can be seen from equation 4.7, in the case of a large error, the adaptive parameter $(\frac{|e(t)|}{\Delta T_{chw,max}})$ tends to be larger; consequently, the hyperbolic term will increase, and as a result, the proportional band will reach its minimum value and will yield a faster temperature response. As the control variable approaches its set-point, the adaptive parameter $(\frac{|e(t)|}{\Delta T_{chw,max}})$ becomes smaller and the hyperbolic term will approach zero. Therefore, the proportional band will reach its maximum value and this will yield a good set-point tracking response. The control parameters used in the experiments are listed in Table 4.2.

Parameter	PB(max)	PB(min)	$k_i(max)$	$\Delta T_{chw,max}$	k_2
Value	1.76	0.44	144s	8	1

Table 4.2 Control parameters for modified gain scheduling adaptive control
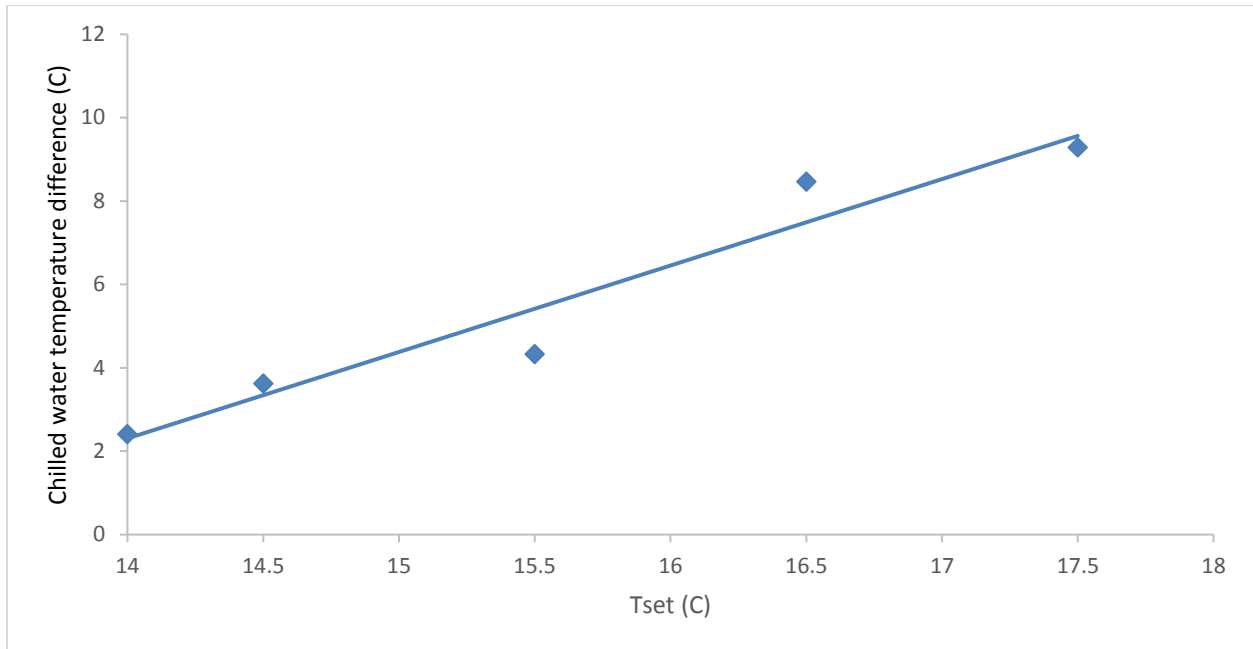
Figure 4.6 Relationship between the set-point (Tset), and the chilled water temperature difference (ΔT_chw)

The dynamic responses of adaptive gain scheduling control under similar load conditions as before are plotted in Figure 4.7. It can be seen from the figure that the AGS control responses are similar to the responses from the GS control. The responses reached the set-point within 450 seconds (from 22°C to 14.5°C). A further change in the set-point by 2°C from a lower to a higher value shows that the responses closely followed the step change and reached a steady state in about 300 seconds. Although the responses from both the AGS and GS control are similar for this particular load condition, the advantage of the AGS control will be apparent when dealing with variable load conditions as discussed in the next section.
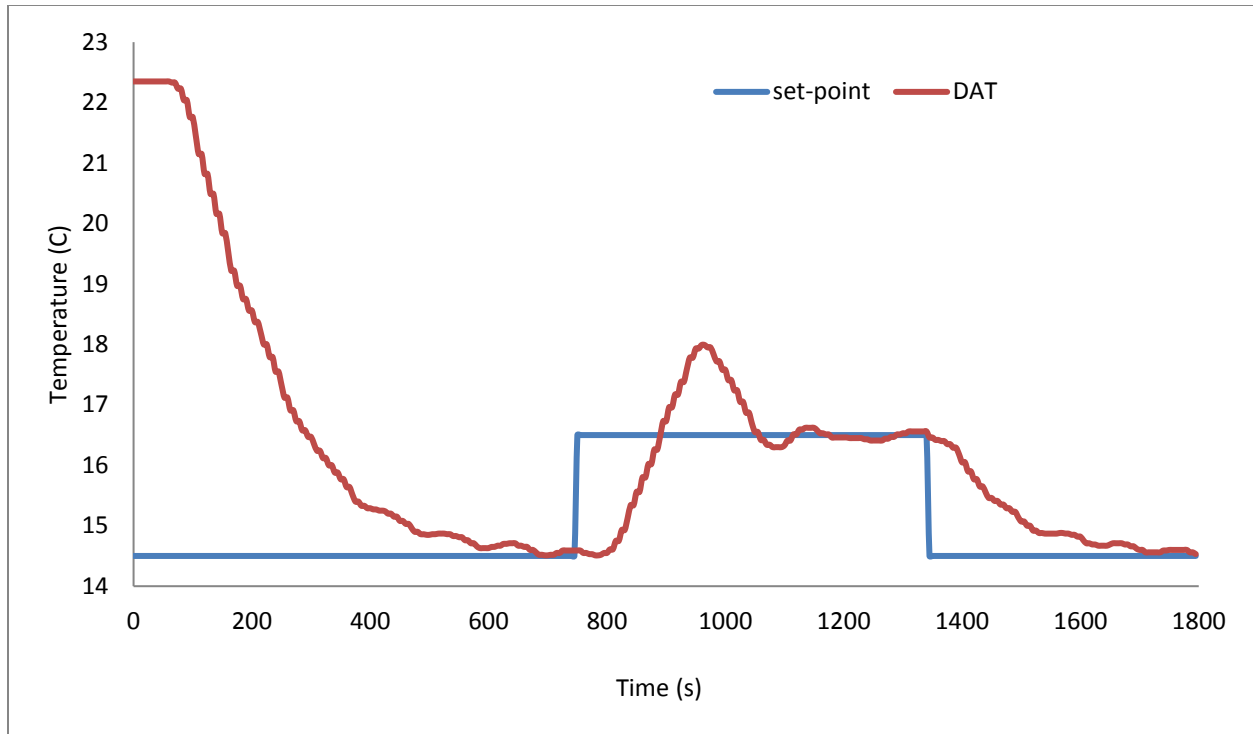
Figure 4.7 Adaptive Gain Scheduling Control for DAT loop due to set-point change

4.4.2 AGS control performance under load disturbances

In real plant operation in buildings, HVAC systems operate under partial load conditions most of the time. Therefore, the system performance under partial load conditions and the effects of sudden load disturbances have to be studied to test the control performance of the system. To this end, experiments have been conducted under the following two scenarios and the results are plotted in Figure 4.8-4.10.

1. A set-point change under partial load (from 15°C to 17°C) for both control methods;
2. A step change in fan speed (1500 RPM to 800 RPM) which corresponds to air flow rate change from 800 CFM to 300 CFM.

Figure 4.8 shows that the new AGS control provides a much better set-point tracking response. The GS control did not converge with the pre-set maximum proportional band (PB(max)=1.76 and PB(min)=0.44). However, the AGS control with the same PB limits was able to track the set-

56

point and reach a steady state within 400 seconds with only 1.2°C overshoot. In other words, for the same proportional band range, the AGS control extended the effective operating range of the control.

Figures 4.9 shows the dynamic responses for both control methods due to a step change under partial load condition and air flow rate change from 800 cfm to 300 cfm. It can be seen that the gain scheduling control method caused significant oscillations and took nearly 25 minutes to reach a stable final value at low load condition. However, the AGS control method reached a steady state within 400 seconds.

Figure 4.10 depicts that the GS control method responses to the disturbance reach a steady state in about 60 seconds with a 0.5°C undershoot and the oscillation is about±0.3°C. On the other hand, the AGS control method reduced the undershoot to 0.3°C and the deviation is only±0.2°C.
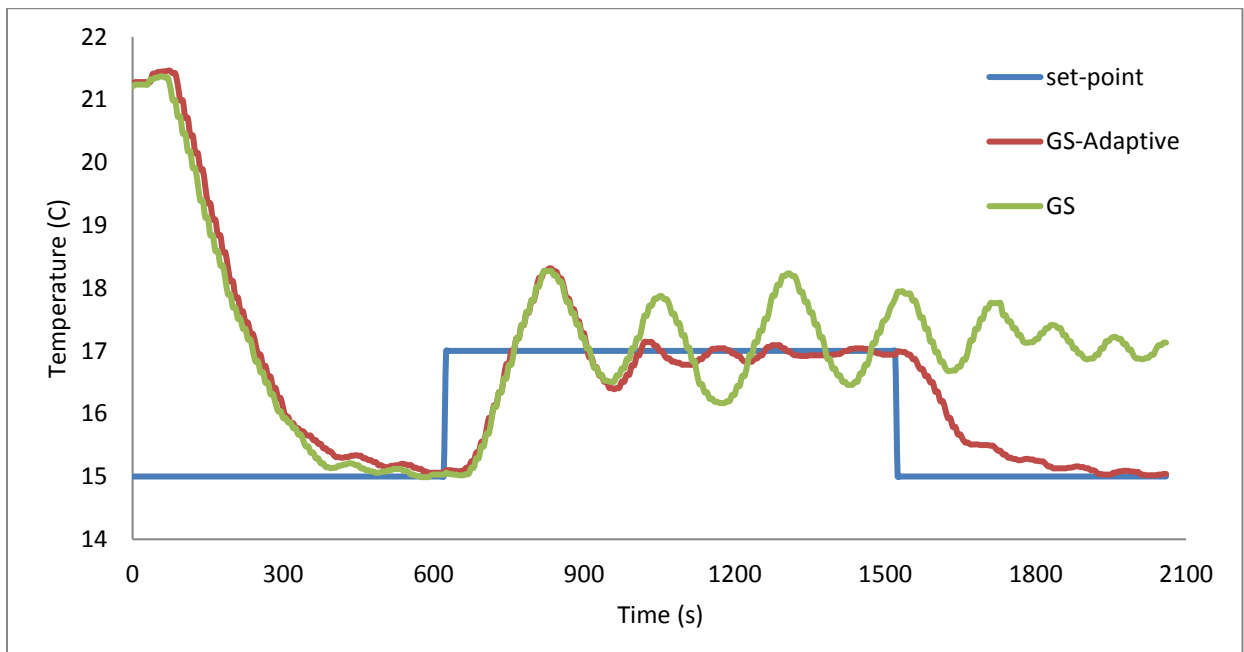
Figure 4.8 Dynamic performance comparison of GS and AGS under partial load with higher set-point (15-17)

57

Figure 4.9 Gain Scheduling control for DAT loop due to load disturbance

Figure 4.10 AGS control for DAT loop due to load disturbance

4.4.3 Modeling and Simulation of AGS control Performance

Compared to experimental studies, model based simulations have inherent advantages which enable fast and cost effective control design. In addition, they can also effectively evaluate the system performance under a wide variety of operating conditions and investigate the feasibility of implementing control strategies. In this thesis the AGS control could not be fully tested due to the fact that the chiller has a built-in on-off control system which cannot be accessed or modified to implement the AGS control defined by Equation 4.8. To this end, the objective was to model and simulate the DAT system and carry out simulation runs to validate the concept of AGS control defined by Equation 4.8. Therefore in this section, the simulation results will be used to check the proof of concept of the AGS control design. The DAT system developed by Zheng (1997) was used and was reconfigured to match the specifications of the DAT system installed in the test facility. The model equations were solved using Matlab. The cooling coil model was a typical counter-cross-flow cooling coil described by the following equations:

For air temperature:

$$\frac{dT_a}{dt} = -\frac{h_t \eta_{s,ov} A_o}{\rho c_v A}(\underline{T_a} - \underline{T_t}) - \frac{\gamma \dot{m}_a}{\rho A L_c}(T_a - T_{a,in}) \qquad \text{(eq. 4.9)}$$

For water temperature:

$$\frac{dT_w}{dt} = \frac{\dot{m}_w}{m_{wL_c}}(T_{chwst} - T_{chwrt}) + \frac{h_{it} A_{it}}{m_w c_w}(\underline{T_t} - \underline{T_w}) \qquad \text{(eq. 4.10)}$$

For tube temperature:

$$\frac{d\underline{T_t}}{dt} = \frac{1 - \eta_s}{\eta_s + \frac{m_t c_t}{m_{fin} c_{fin}}}\{\frac{\gamma \dot{m}_a}{\rho A L_c}(T_a - T_{a,in}) -$$

$$\frac{h_{it} A_{it}}{m_{fin} c_{fin}(1 - \eta_s)}(\underline{T_t} - \underline{T_w}) + (\frac{h_t \eta_{s,ov} A_o}{\rho c_v A} + \frac{\eta_{s,ov} h_c A_o}{m_{fin} c_{fin}(1 - \eta_s)})(\underline{T_a} - \underline{T_t})\} \qquad \text{(eq. 4.11)}$$

where $T_a, T_{a,in}, and \ \underline{T_a}$ are the air leaving, entering and the mean bulk temperatures of two adjacent control volumes; $T_{chwrt}, T_{chwst}, and \ \underline{T_w}$ are the water leaving, entering and the mean

bulk temperatures of two adjacent control volumes; $\underline{T_t}$ is the mean bulk tube wall temperature; $\dot{m}_w$ and $\dot{m}_a$ are the mass flowrate of the water and air; m_w, m_t, and m_{fin} are the mass of water, tube, and fin per unit length; c_v, c_w, c_t, and c_{fin} are the specific heats of air, water, tube and fin materials; h_t and h_{it} are the heat transfer coefficients; A_o, and A_{it} are the total air-side and water-side heat transfer surface areas; A is the minimum sectional air flow area; L_c is the coil depth and η_s and $\eta_{s,ov}$ are the fin and overall efficiency respectively.

The design parameters of the coil installed in the experimental facility were used and the equations to calculate heat transfer coefficients, heat transfer area and efficiency were adapted from McQuiston (2000).

The coil is divided into four control volumes for each row of the tube and the dynamic equations are applied to each control volume. It is assumed that the air temperature, chilled water temperature and tube wall temperature in each control volume are uniformly distributed.

The AGS control algorithm was applied and is described by the following equation:

$$PB(t) = PB(max) - (PB(max) - PB(min))tanh\left(\frac{|e(t)|}{\Delta T_{chw}}|e(t)|\right) \qquad \text{(eq. 4.8)}$$

$$k_i(t) = k_i(max)(1 - tanh(k_2|e(t)|)) \qquad \text{(eq. 4.5)}$$

where

ΔT_{chw} is chilled water temperature difference between the return water temperature and supply water temperature.

The simulation results are depicted in Figures 4.11-4.12. The response of the adaptively controlled system due to a set-point change is shown in Figure 4.11. Compared to the real plant performance, the adaptive control simulation provides a rapid and stable response to a 2 degree set point change as the chilled water supply temperature remained constant at 7 ^{0}C. Figure 4.12 shows the dynamic response of the adaptively controlled system due to a change in air flow rate from 800 CFM to 300 CFM. Compared to the real experimental results, the simulation results give a much faster and

60

more stable dynamic response to the disturbance since the chilled water supply and return temperature are more stable, as shown in the figures. It can be reasoned from these simulation results that the AGS control adapts to load changes rapidly and provides smooth and stable control.
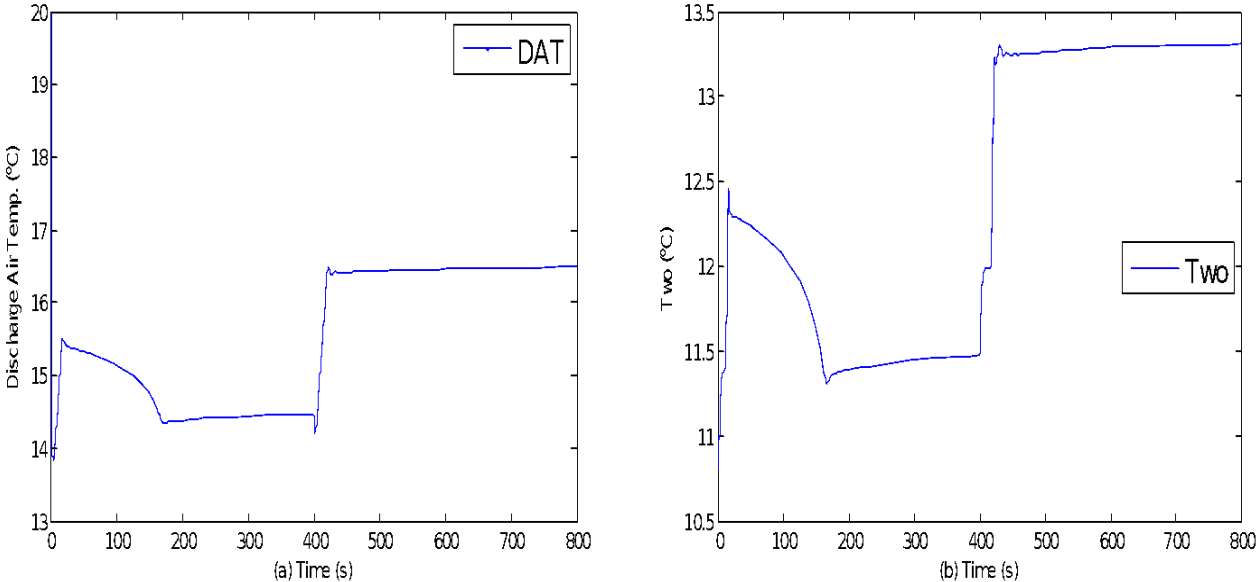
Figure 4.11 AGS control for DAT loop due to set-point change (14.5℃-16.5℃)
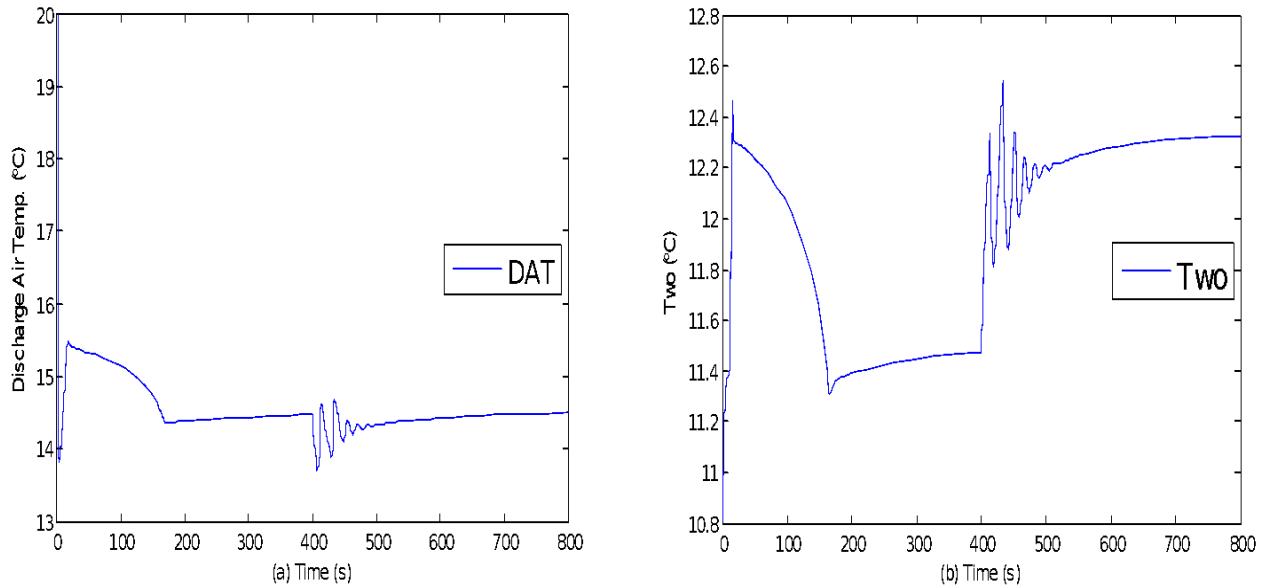
Figure 4.12 AGS control for DAT loop due to air flow rate disturbance (800 CFM to 300 CFM)

4.5 Summary and Conclusions

The control performance of the discharge air temperature loop was assessed by the Ziegler-Nichols method, the gain scheduling control method and a new adaptive gain scheduling control method. The steady state time for the system to reach 14.5℃ from an initial condition of 22℃ was nearly the same (400 seconds) for all three control modes. However, the results showed a different response to a set-point change of 2℃. The Ziegler-Nichols method could not reach a steady state. The gain scheduling control method and adaptive control method were able to reach a steady state in about 400 seconds. However, it was found that the gain scheduling control method caused significant oscillations and took nearly 25 minutes to reach a stable final value. On the other hand, the adaptive gain scheduling control displayed good control performance by extending the effective control range of the system to wide variations in load disturbances. A DAT system model with AGS control was developed. The model equations were simulated to study the control performance of the system with the adaptive parameter ($\frac{|e(t)|}{\Delta T_{chw}}$) under different

62

load disturbances. The simulation results validate the proof of concept and the results show that the adaptive gain scheduling control provides a rapid and stable control performance under different load scenarios.

CHAPTER 5　　Control Loop Interactions and Optimal Operation by Adaptive Gain Scheduling Control

5.1 Introduction

Control loop interactions often occur in multi-loop dynamic systems. A change in the control parameters of one loop also affects the dynamic responses of the other loops. This is likely to increase the energy consumption of HVAC systems. To better understand the control loop interactions in a dual-duct system, oscillations were introduced in the control loop and their effects on the other control loops were examined. Interactions in the following control loops of the dual-duct system were investigated.

1. Cooling coil discharge air temperature control loop (valve actuator)
2. Heating coil discharge air temperature control loop
3. Mixed air temperature control loop (damper actuator)

The experimental results show that significant interactions occur among the control loops. In other words, the affected control loops require retuning to improve the system performance. To this end, the adaptive gain scheduling tuning method developed in the previous chapter was applied on the affected control loops to reduce the oscillations and improve the system performance.

In this chapter, the following topics will be discussed: (i) the interaction between control loops will be ranked by defining an impact factor, (ii) the degree of the interactions between control loops under AGS control will be determined and (iii) the interactions under conventional PI control and AGS control will be compared.

5.2 Loop interactions under poorly tuned PI controllers

5.2.1 Entire system response under real operating conditions

The system was operated under full load conditions (fan speed=1500 RPM) to determine the dynamic performance of the three control loops working simultaneously in the dual-duct system. Each controller was tuned according to the Zigeler-Nichols method (control parameters shown in Table 5.1). To perform this test, the following conditions were maintained before the operation: the cold duct damper was fully opened and the hot duct damper was half opened (400 CFM in the hot duct and 500CFM in the cold duct), the average chilled water supply temperature was 7°C and the fan speed was maintained at 1500 RPM.

Figure 5.1 shows the system response with conventional PI control as the base case control performance. It can be seen from the figure that the cooling coil discharge air temperature reaches its set-point value of 15°C within 300 seconds. After the initial transient response, the system outputs reached stable values.

To measure the degree of interactions between control loops, the PB was changed until oscillations were induced in one control loop at a time. Its impact on the remaining control loops was quantified by defining an impact factor, which is the ratio of temperature difference to the proportional band difference expressed by the following equation:

$$Impact\ factor = \frac{\Delta T}{\Delta PB}$$
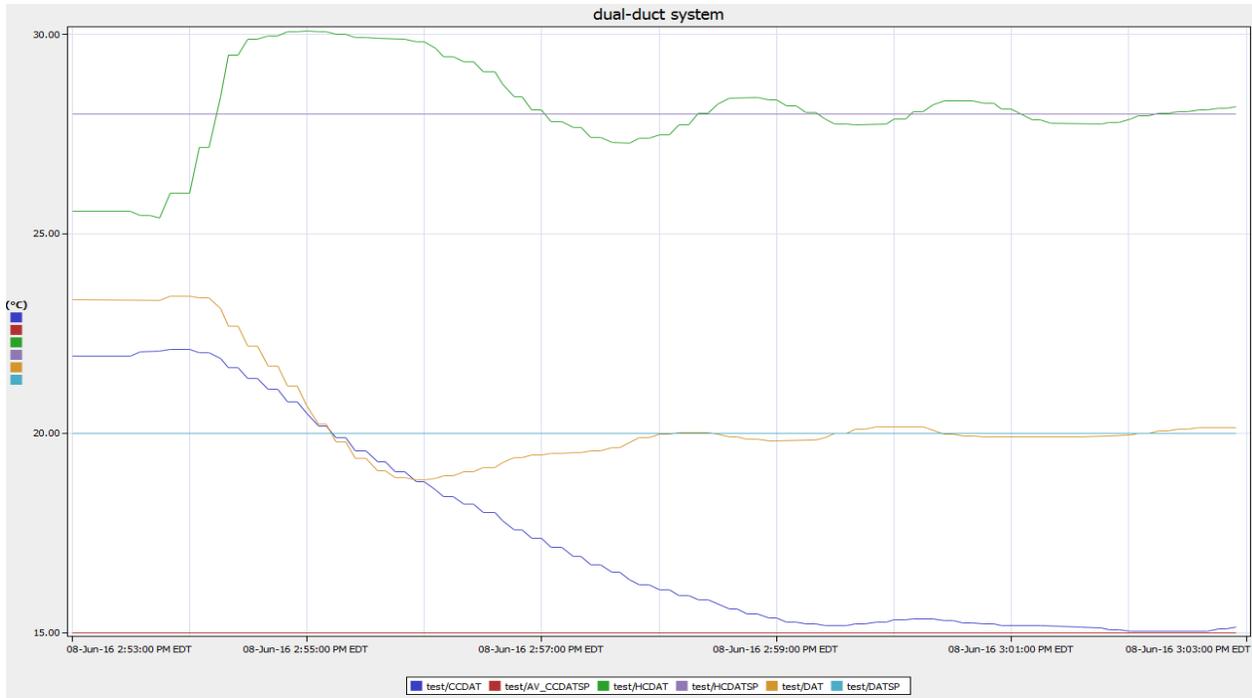
Figure 5.1 Fine-tuned dual-duct system with conventional PI control

Tuning parameters	Valve controller	Damper controller	Heater controller
PB	0.75	2	3.5
Ti (seconds)	144	160	50

Table 5.1 PI Control parameters

5.2.2 Loop interactions under poorly tuned valve actuator

In order to induce continuous oscillations in the cooling coil discharge air temperature loop, the proportional band was reduced from 0.75 to 0.05 while the integral time was kept constant. The dynamic response of the entire system is plotted in Figure 5.2. The responses show that the oscillations in cooling coil discharge air temperature also affect both the mixed air temperature and the heating coil discharge air temperature. The combined effects result in an unstable system with irregular control loop responses. The mixed air temperature has a maximum temperature difference of $\pm0.8°C$ and the heating coil discharge air temperature has a maximum temperature difference of $+1°C/-1.4°C$. The impact factor of the poorly tuned valve actuator on the other two

66

loops was determined:

Impact on the mixed air temperature loop:

$$impact\ factor = \frac{\Delta T}{\Delta PB} = \frac{1.6 - 0}{0.75 - 0.05} = 2.29°C/unitPB$$

Impact on the heating coil discharge air temperature:

$$impact\ factor = \frac{\Delta T}{\Delta PB} = \frac{2.4 - 0.4}{0.75 - 0.05} = 2.86°C/unitPB$$
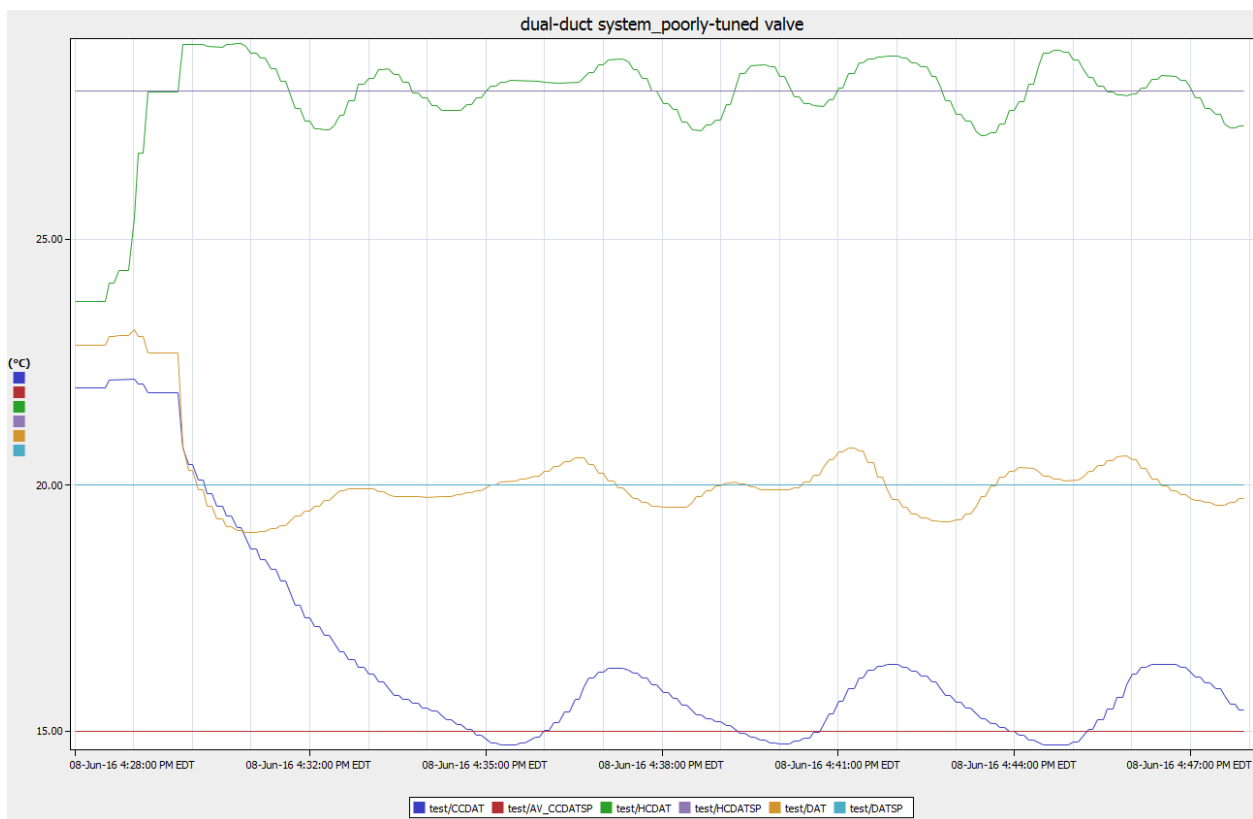
Figure 5.2 Dynamic response under poorly tuned valve actuator

5.2.3 Loop interactions under poorly tuned heater controller

To introduce a continuous period of oscillations in the heating coil discharge air temperature

67

loop, the proportion band was decreased from 3.5 to 0.2 and the integral time was kept constant. The resulting dynamic responses of the entire system are plotted in Figure 5.3. The results show that the over sensitive controller produced continuous oscillations in the heating coil temperature responses and impacted the mixed air temperature responses. However, the interactions were small, with a temperature difference of+0.3℃/−0.2℃. Furthermore, the poorly tuned heater controller does not seem to influence the cooling coil discharge air temperature control.

The impact factors of the poorly tuned heater controller on the other two loops are summarized below:

Impact on the mixed air temperature loop:

$$impact\ factor = \frac{\Delta T}{\Delta PB} = \frac{0.5 - 0}{3.5 - 0.2} = 0.15℃/unitPB$$

Impact on the cooling coil discharge air temperature:

$$impact\ factor = \frac{\Delta T}{\Delta PB} = \frac{0.2 - 0}{3.5 - 0.2} = 0.06℃/unitPB$$
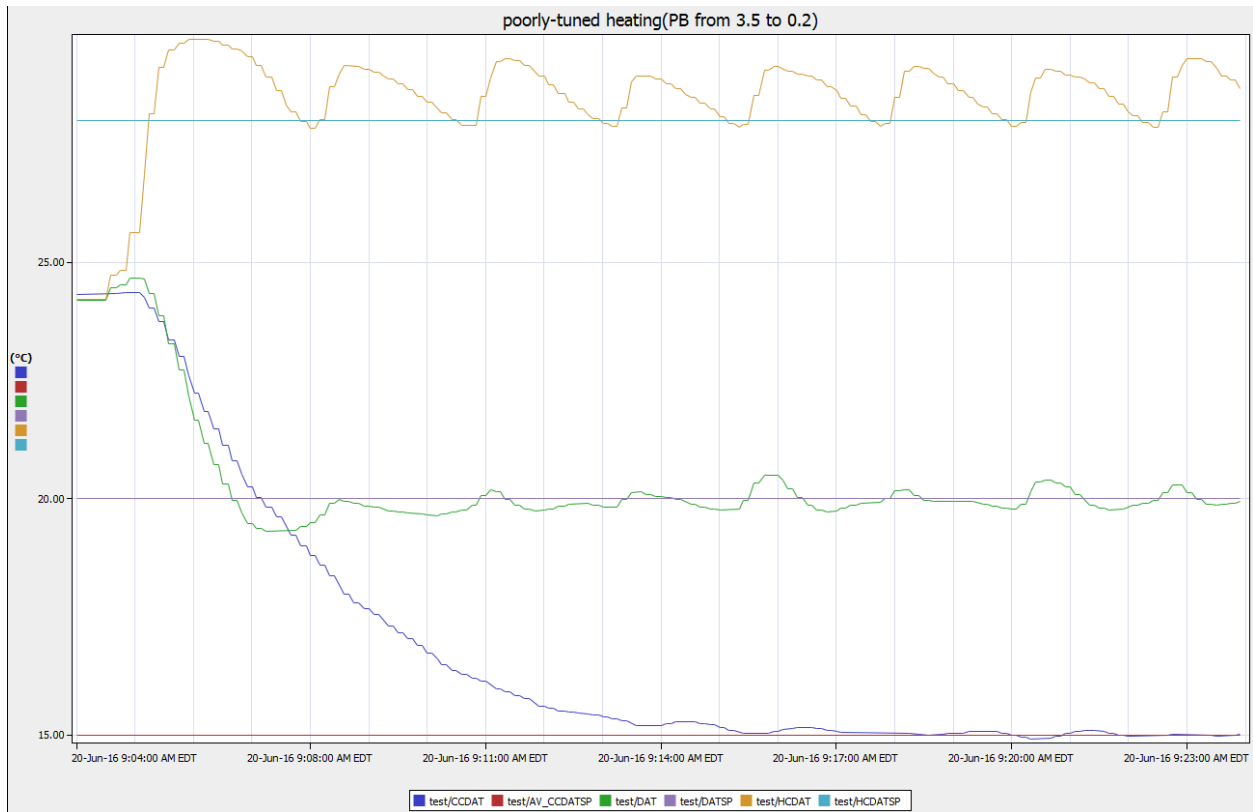
Figure 5.3 Dynamic response under poorly tuned heater controller

5.2.4 Loop interactions under poorly tuned damper actuator

The proportional band of the mixed air control loop was decreased from 2 to 0.1 to introduce continuous oscillations in the control loop. The resulting system responses were plotted in Figure 5.4. The responses show that a poorly tuned damper actuator control impacts both the hot and cold duct temperature control loops. The heating coil discharge air temperature variations recorded were $+1℃/-0.8℃$ and the cooling coil discharge air temperature variations ranged between $+1.5℃/-0.5℃$. As a result, the mixed air temperature had a 2.2℃ overshoot and a 1.2℃ undershoot.

The impact factors on the other two loops due to the poorly tuned damper actuator are given below.

69

Impact on the heating coil discharge air temperature loop:

$$impact\ factor = \frac{\Delta T}{\Delta PB} = \frac{1.8 - 0.4}{2 - 0.1} = 0.74°C/unitPB$$

Impact on the cooling coil discharge air temperature:

$$impact\ factor = \frac{\Delta T}{\Delta PB} = \frac{2 - 0.2}{2 - 0.1} = 0.95°C/unitPB$$
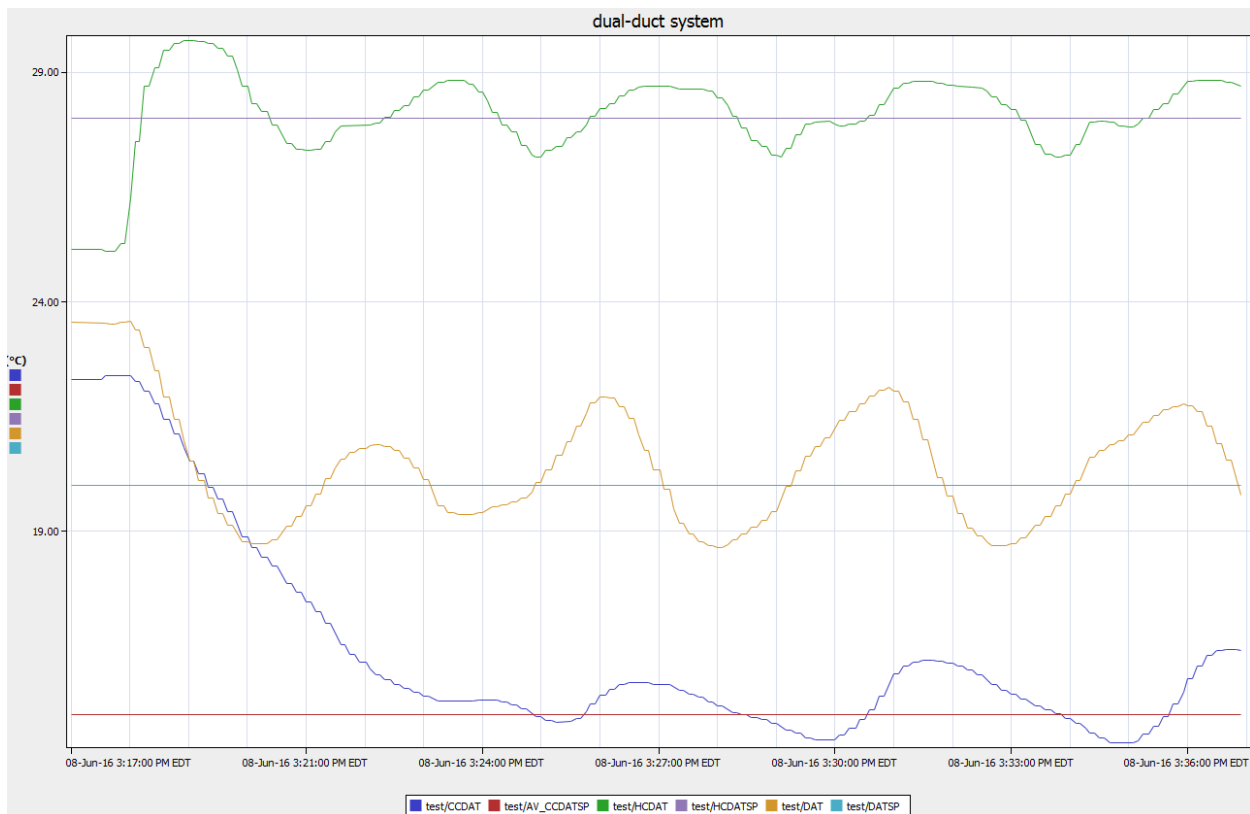

Figure 5.4 Dynamic response under poorly tuned damper actuator

From these observations, it can be concluded that:

1. An oscillatory mixed air temperature control loop impacts both hot and cold discharge air temperature loops, showing sustained oscillations;

2. A poorly tuned cooling coil discharge air temperature loop significantly impacts the heating

70

coil and mixed air temperature control loops. The affected control loop responses showed delayed and irregular pattern oscillations;

3. A poorly tuned heating coil discharge air temperature loop does not significantly impact the mixed air and cooling coil discharge air control loop responses;

4. The critical control loops, in order of the severity of their impact factors, are (i) the cooling coil discharge air temperature loop, (ii) the mixed air temperature loop and (iii) the heating coil discharge air temperature loop. In other words, adaptive control of the control loop should be an important consideration in realizing good control performance of HVAC systems.

5.3 Loop interaction under adaptive gain scheduling control

According to the observations made in section 5.2, loop interactions occur between control loops with poorly tuned controllers. Therefore, the adaptive gain scheduling control developed in chapter 4 will be a good candidate control to reduce the control loop interactions. Since the heating coil air temperature loop does not greatly influence the other loops, it was not considered in this section. The tests were conducted by applying the AGS control to the discharge air and mixed air temperature control loops one at a time. The purpose of this series of experiments is to check the feasibility of optimizing the system performance by only applying AGS control to the most critical loop in the system.

5.3.1 Loop interactions under adaptive gain scheduling control of valve actuator

Figure 5.5 shows the system responses with an adaptive gain scheduling valve controller and a poorly tuned damper controller. In the test conducted, the adaptive gain scheduling control method (equations 4.5 and 4.7) was applied to the valve control and the control parameters were shown in Table 5.2. The damper controller was poorly tuned by decreasing the proportional band from 2 to 0.1.

71

The figure 5.5 depicts the responses of oversensitive damper controllers, which cause continuous periods of oscillations in the mixed air temperature and heating coil discharge air temperature. However, it can be seen from the figure that the adaptive gain scheduling valve control was working properly to keep the cooling coil discharge air temperature within an acceptable range (±0.2°C). Also, compared to the responses in Figure 5.4, the gain scheduling valve controller reduced the amplitude of the oscillation on the mixed air temperature from +2.2°C/−1.5°C to +1.2°C/−1.0°C, while the heating coil discharge air temperature ranged between +0.7°C/ −0.5°C.

Parameter	PB(max)	PB(min)	$k_i(max)$	$\Delta T_{chw,max}$	k_2
Value	1.76	0.44	144s	8	1

Table 5.2 Adaptive gain scheduling control parameters for valve controller
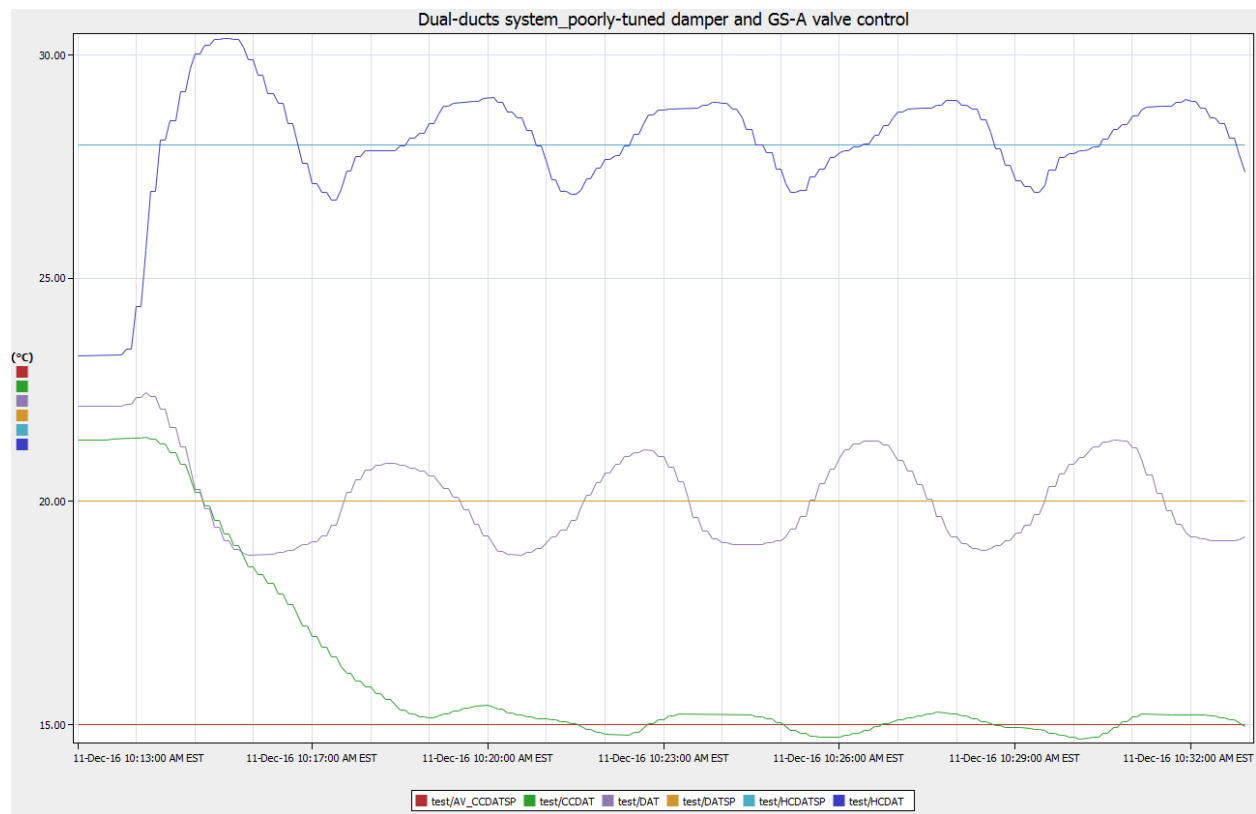
Figure 5.5 Dynamic response with adaptive gain scheduling valve control and poorly tuned damper controller

72

5.3.2 Loop interactions under adaptive gain scheduling damper control

Figure 5.6 shows the system responses with the adaptive gain scheduling damper controller and poorly tuned valve controller. To perform this test, the adaptive gain scheduling method (equation 4.5 and 4.7) was applied to the damper control loop with the control parameters listed in Table 5.3. The damper controller was badly tuned by decreasing the proportional band from 0.75 to 0.05.

The results depicted in Figure 5.6 indicate that the poorly tuned controller caused continuous oscillations in the cooling coil discharge air temperature, which also affected both the mixed air temperature and the heating coil discharge air temperature. It can be seen from the figure that the mixed air temperature was fluctuating with a maximum temperature difference of $\pm0.8°C$ and the heating coil discharge air temperature was also fluctuating with a maximum temperature difference of $\pm0.8°C$.

Parameter	PB(max)	PB(min)	$k_i(max)$	$\Delta T_{chw,max}$	k_2
Value	2.6	1.7	160s	8	1

Table 5.3 Gain scheduling-adaptive control parameters for damper controller
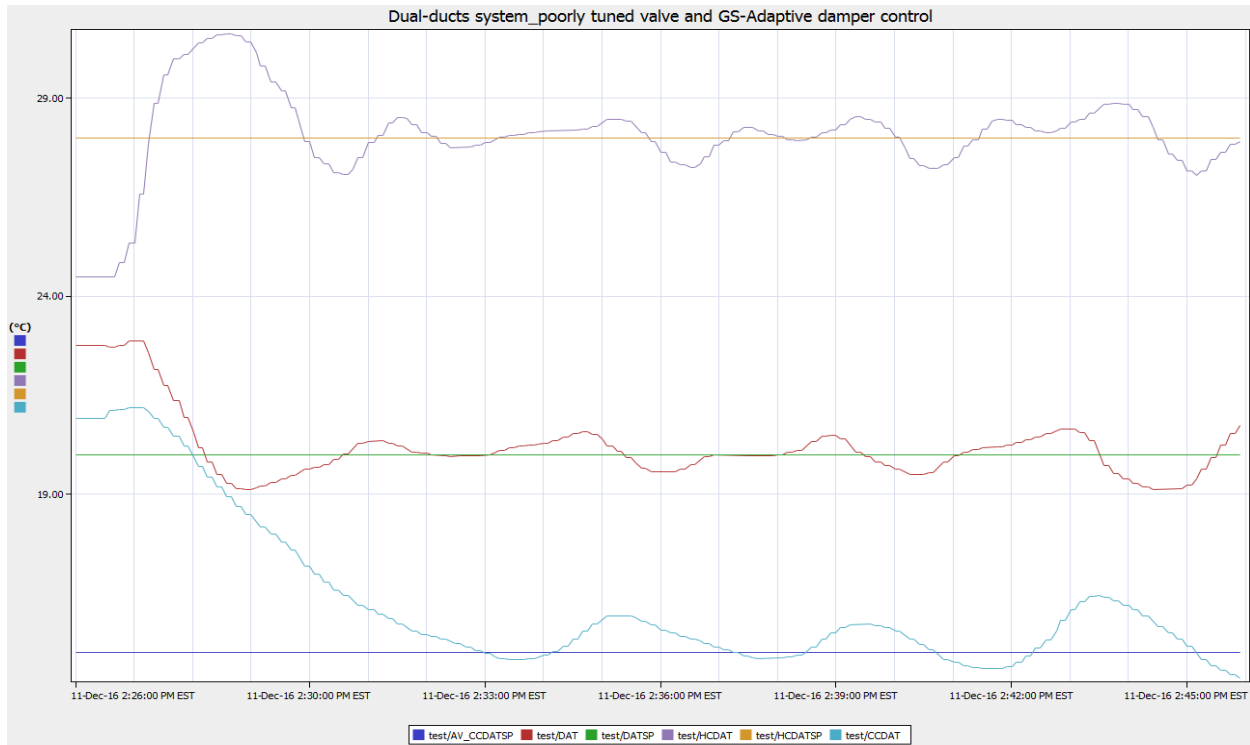
Figure 5.6 Dynamic response with adaptive gain scheduling damper control and poorly tuned valve controller

5.3.3 System responses optimized by adaptive gain scheduling control

The dynamic performance of the dual-dual system was optimized by applying the adaptive gain scheduling control. The adaptive gain scheduling control was applied to the entire system with the exception of the heating coil loop, since this loop does not interact with others. The control parameters of each controller are summarized in Tables 5.2 and 5.3.

The dual duct system responses with adaptive gain scheduling control are plotted in Figure 5.7. The responses show that the AGS control works perfectly to control all three loops to their respective set-points. Compared to the conventional PI control responses (section 5.2.1), the time for the mixed air temperature loop to reach a steady state reduced from 240 seconds to 200 seconds and the undershoot was also reduced to 0.5℃.

74
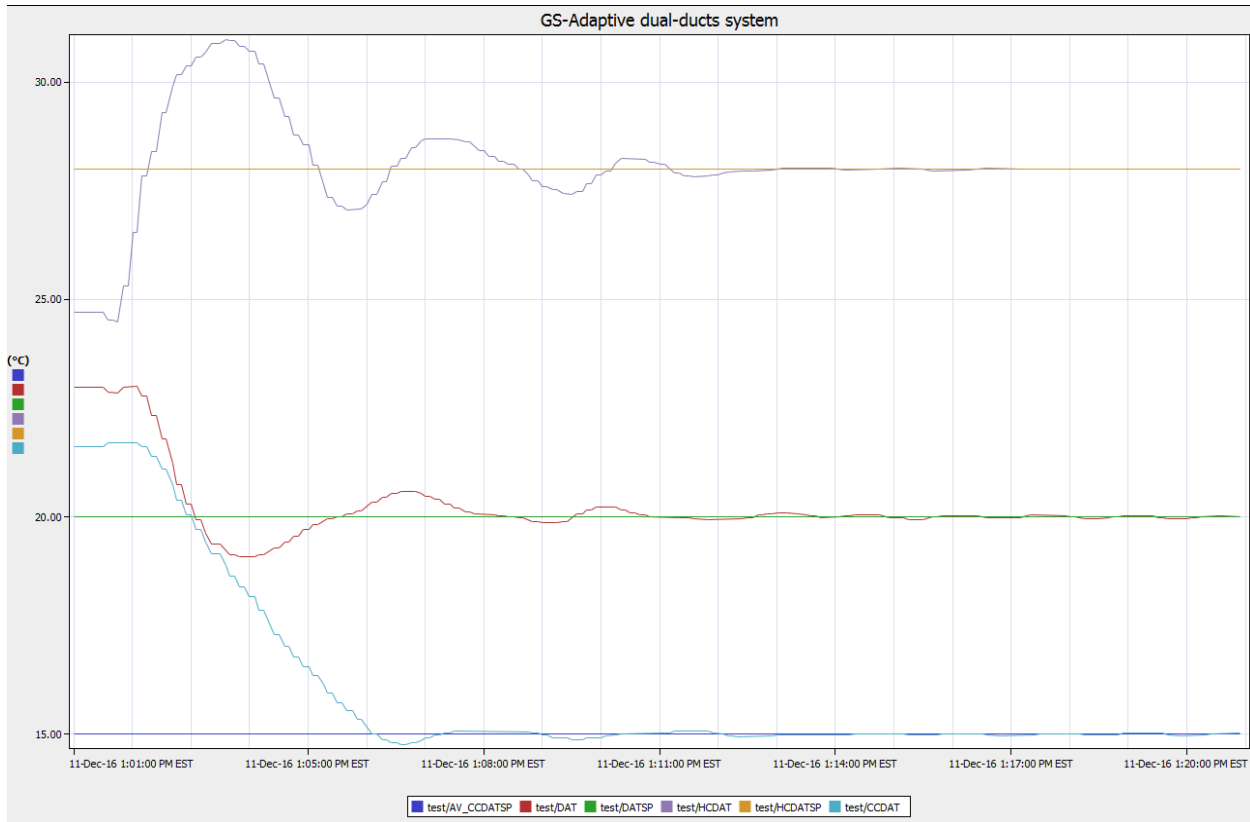
Figure 5.7 Dynamic response with gain scheduling-adaptive valve and damper control

To determine the effectiveness of reducing loop interaction with adaptive gain scheduling control, the impact factors were calculated based on the results presented in section 5.3. The results were compared with the base case with conventional PI control.

1. With the valve actuator under adaptive gain scheduling control mode, determine the impact factor of the poorly tuned damper actuator on the other two control loops

   Impact on the cooling coil discharge air temperature:

$$impact\ factor = \frac{\Delta T}{\Delta PB} = \frac{0.4 - 0}{2 - 0.1} = 0.21°C/unitPB$$

   Impact on the heating coil discharge air temperature:

$$impact\ factor = \frac{\Delta T}{\Delta PB} = \frac{1.2 - 0}{2 - 0.1} = 0.63°C/unitPB$$

75

2. With the damper actuator under adaptive gain scheduling control mode, determine the impact factor of the poorly tuned valve actuator on the other two loops

Impact on the mixed air temperature:

$$impact\ factor = \frac{\Delta T}{\Delta PB} = \frac{1.6 - 0}{0.75 - 0.05} = 2.29°C/unitPB$$

Impact on the heating coil discharge air temperature:

$$impact\ factor = \frac{\Delta T}{\Delta PB} = \frac{1.6 - 0}{0.75 - 0.05} = 2.29°C/unitPB$$

By comparing the results with the original cases, it can be concluded that:

1. With the adaptive gain scheduling valve controller, the impact factor of the poorly tuned damper controller on the other two loops was reduced from $0.95°C/unitPB$ and $0.74°C/unitPB$ to $0.21°C/unitPB$ and $0.63°C/unitPB$ respectively. Therefore, the adaptive gain scheduling valve controller reduces the loop interactions caused by a poorly tuned system.

2. With the adaptive gain scheduling damper controller, the impact factor of the poorly tuned valve controller on the other two loops remained the same as in the original PI control. This shows that the adaptive gain scheduling of the damper controller does not improve the loop interaction caused by a poorly tuned valve controller. To improve system performance, both control loops have to be controlled using AGS control.

5.4 Summary and conclusion

The dual-duct system was operated under both the conventional PI and adaptive gain scheduling controls. The experimental results showed that the dynamic performance of a system with the adaptive gain scheduling control is better than that of one with the conventional PI control, giving shorter settling time and less undershoot. An impact factor was defined to quantify the impact of loop interactions. It was found that the cooling coil discharge air temperature loop exerts a major influence on the mixed air and heating coil discharge air temperature loops. The

next loop, in terms of its severity of impact, was the mixed air temperature control loop which affected both the cooling and heating coil discharge air temperature loops. It was found that the heating coil discharge air temperature loop does impact the cooling coil discharge air and the mixed air temperature control loops.

The impact factors were also determined to evaluate the impact of a poorly tuned control loop on the adaptive gain scheduling control loop. In the case of an adaptive gain scheduling valve controller and a poorly tuned damper controller, the AGS valve controller improved the loop interaction by reducing the amplitudes of the other loops, which resulted in low impact factors. However, the adaptive gain scheduling damper controller was not found to improve the loop interactions caused by a poorly tuned valve controller, which also verifies the critical nature of the cooling coil valve controller in dual duct system operation.

CHAPTER 6   Conclusions and Future Work

An experimental study of tuning method application and development was conducted on a laboratory dual-duct system. The test facility consisted of three local control loops. Both individual control loop performance and the loop interactions were analyzed. The prioritization of control loop due to loop interactions was evaluated and the gain scheduling-adaptive tuning method was applied to the entire system to optimize the system responses caused by loop interactions.

6.1 Summary and conclusion of the study

6.1.1 System dynamic performance in open-loop

A series of open loop tests were conducted to identify the steady state characteristics and dynamic performance of the following three sub-systems: (i) the air flow sub-system, (ii) the water distribution sub-system and (iii) the discharge air system. From the open loop test results, the system's mechanical and thermal dynamic performance, such as operational range, and actuator effective operational range, were identified. These parameters helped in the study of the dynamic performance of the overall system. Through the test results, the following conclusions were generated:

1. The air flow rate is almost linearly related to the damper position and the maximum flow rates in the cold and hot ducts are 757 CFM and 936 CFM respectively.
2. The steady state time of the airflow sub-system for 100%, 75%, 50% and 25% damper opening are 180 seconds, 140 seconds, 100 seconds and 70 seconds respectively.
3. In this test facility, it was found that a large hot air duct damper opening and a small cold air duct damper opening could lead to zero air flow in the cold air duct. It is therefore better to control the mixed air temperature through the hot duct damper.

4. The operational range of the chilled water three-way valve is between 40% and 100%, the maximum chilled water flow rate was found to be 6 GPM and the steady state time is 100 seconds.

5. The discharge air temperature reaches a steady state within about 600s under various load conditions.

6. The controllable discharge air temperature range is between 14℃ and 17.5℃ under full load conditions and the lowest discharge air temperature reached was 11℃.

7. Since the chiller is controlled by the manufacturer's built-in control system, it was observed that the chilled water supply temperature supplied by the chiller fluctuated between 8.1℃ and 5.5℃ when the set-point was set at 7℃.

8. The dead time of all control loops in the system was found to be about 30 seconds.

6.1.2 Controller design methods and closed-loop responses of the control loops

The discharge air temperature loop was tuned using the Ziegler-Nichols method, the gain scheduling PI control method and a new adaptive gain scheduling control method. The steady state time for the DAT system to reach the set-point from the same initial conditions was found to be about 400 seconds in all three control methods. However, when a 2℃ change in the set-point was executed, the Ziegler-Nichols method with constant gains failed to steer the temperature response to the new set-point. On the other hand, both the gain scheduling (GS) control and adaptive gain scheduling (AGS) control temperature responses converged to the new point and reached a steady state in about 400 seconds. The advantage of the AGS control over the GS control was that the AGS control extended the good control over a wide range of load conditions, particularly under low load conditions.

An AGS control algorithm is proposed in this thesis. The AGS controller updates the proportional band (PB) based on an adaptive parameter defined by the ratio ($\frac{|e(t)|}{\Delta T_{chw}}$). However, due to the limitations of the test facility, in which the chilled water temperature fluctuated in a cyclical manner, it was necessary to minimize this impact by modifying the adaptive parameter

79

as ($\frac{|e(t)|}{\Delta T_{chw,max}}$). Note that the difference between the two adaptive parameters is the use of the maximum difference in chilled water temperature in the denominator term rather than the instantaneous difference.

Since the AGS control with the adaptive parameter ($\frac{|e(t)|}{\Delta T_{chw}}$) could not be tested in the test facility, it was decided to test its feasibility by conducting a simulation study. To this end, a dynamic model of the DAT system with AGS control was simulated in the Matlab platform to verify the performance of the AGS control with the adaptive parameter ($\frac{|e(t)|}{\Delta T_{chw}}$) under different load disturbances. The simulation results showed that the AGS control gives rapid and stable control responses under different load scenarios.

6.1.3 Control loop interactions

The dual-duct system was operated under both conventional PI and AGS control modes. The experimental results showed that the dynamic performance of the system with AGS is better than the conventional PI method, with shorter settling time and less undershoot.

An impact factor was defined to quantify the impact of control interactions and identify and rank the loops in order of their impacts. The control loop interaction tests were conducted using the conventional PI control and letting one control loop at a time be poorly tuned and recording its impact on the other control loops. It was found that the cooling coil discharge air temperature loop has a major influence on the hot duct temperature control loop and the mixed air temperature control loop. The next in line was the mixed air temperature control loop, which affected the hot and the cold air discharge air temperature loops. It was found that the heating coil discharge air temperature loop did not appreciably impact the other loops.

The impact factor tests were also conducted to evaluate the performance AGS control by letting one control loop at a time in the system be poorly tuned. In the case of AGS control of a valve actuator controller with a poorly tuned damper controller, it was found that the AGS valve actuator controller reduced the loop interactions. The amplitude output temperatures in the hot

and mixed air control loops were reduced, which was reflected by the lower impact factors. However, the AGS damper controller does not reduce the loop interactions caused by a poorly tuned valve controller. This result further confirms that the cooling coil valve control loop remains the most critical control loop in the overall operation of the dual duct system.

6.2 Future work recommendations

The following subjects could be pursued as part of future work:

1. Consideration should be given to energy efficiency along with good control performance. This issue needs to be studied for both the conventional PI control and adaptive gain scheduling control.
2. It is important to include humidity control in the system and study the performance of adaptive gain scheduling control with humidity control.
3. Implementation of the adaptive gain scheduling control in large-scale real-building HVAC systems needs to be studied to validate it's performance under real building operating conditions.

REFERENCES

[1] McCullagh, K.R., Green, G.H., and Chandra, S.S. 1969. An analysis of chilled water cooling dehumidifying coils using dynamic relationships. *ASHRAE Transactions* 75(2):200–09.

[2] Clark, D.R. 1985. Type 12: Cooling or dehumidifying coil. *HVACSIM+ Reference Manual*. National Bureau of Standards (now NIST), Gaithersburg, MD, pp. 63–68.

[3] Elmahdy, A.H., and Mitalas, G.P., 1977. A simple model for cooling and dehumidifying coils for use in calculating energy requirements for buildings. *ASHRAE Transactions* 83(2):103–17.

[4] Zheng, G.R. 1997. Dynamic Modeling and Global Optimal Operation of Multizone Variable Air Volume HVAC System. Ph.D Dissertation, Concordia University, Montreal, Canada

[5] Wang, Y.W., Cai, W.J., et al. 2004. A simplified modeling of cooling coils for control and optimization of HVAC systems. Energy Conversion and Managements 45 (2004) 2915-2930.

[6] Jin, G.Y., Cai, W.J., Wang, Y.W., and Yao, Y. 2006. A simple dynamic model of cooling coil unit. Energy Conversion and Managements 47 (2006) 2659-2672.

[7] Yao, Y., and Liu, S.Q. 2008. The transfer function model for dynamic response of wet cooling coils. Energy Conversion and Managements 49 (2008) 3612-3621.

[8] Zheng, G.R., and Zaheer-uddin, M., 1999. Discharge air system: modeling and optimal control. International Journal of Energy Research 23 727-738 (1999).

[9] Tashtoush, B., Molhim, M., and Al-Rousan, M., 2005. Dynamic model of an HVAC sytem for control analysis. Energy 30 (2005) 1729-1745.

[10] Robinson, K.D. 1998. Damper control characteristics and mixing effectiveness of an air-handing unit combination mixing/filter box. ASHRAE Transactions 104(1998): 629.

[11] Becelaera, R.V., Sauer, H.J., and Finaish, F. 2005. Flow resistance characteristics of air flow control dampers. HVAC&R Research. January 2005 Volume 11.

[12] Fruehauf, P. S., Chien, I.L., and Lauritsen, M. D., ISA. 1994. Simplified IMC-PID tuning rules.Trans. 1994, 33, 43-59.

[13] Skogestad, S. (2003). Simple analytic rules for model reduction and PID controller tuning. *Journal of Process Control, 13*(4), 291-309.

[14] Ruel. M., 2000. A simple method to determine control valve performance and its impacts on control loop performance. Top Control Inc.

[15] Ãstrom, K. J., & HÃgglund, T. (2004). Revisiting the Ziegler-Nichols step response method for PID control. *Journal of Process Control, 14*(6), 635-650.

[16] Zhou., John Q., Claridge, David E., 2012. PI tuning and robustness analysis for air handler discharge air temperature control. Energy and Building. 44 (2012) 1-6.

[17] Lin, M. G., Lakshminarayanan, S., and Rangaiah, G. P. (2008). A comparative study of recent/popular PID tuning rules for stable, first-order plus dead time, single-input single-output processes. *Industrial and Engineering Chemistry Research, 47*(2), 344-368.

[18] Yamakawa, Y., Kamimura, K., Yamazaki, T., & Kurosu, S. (2009). Stability of temperature control in VAV systems. *ASHRAE Transactions, 115*(1), 613-621.

[19] Jette, I., Zaheeruddin M., and Fazio, P. PI-control of dual duct systems: manual tuning and control loop interaction. Energy Convers. Mgmt Vol. 39, No. 14, pp. 1471-1482, 1998

[20] Matusu, R., & Prokop, R. (2010). Experimental verification of design methods for conventional PI/PID controllers. *WSEAS Transactions on Systems and Control, 5*(5), 269-280.

[21] Warren, R. D., Navale, R. L., Nelson, R. M., & Klassen, C. J. (2009). Experimental measurement and uncertainty analysis on the energy performance of a chilled water cooling coil. *, 115 PART 2* 676-688.

[22] Sedaghati, A. (2006), A PI controller based on gain scheduling for synchronous generator. Turk J Elec Engin, VOL.14, NO.2 2006

[23] Zaky, M.S. and Ismaeil, E.M. (2008) Gain scheduling adaptive PI control of Hybrid Stepper Motor drives. Proceedings of the 14th International Middle East Power Systems Conference (MEPCON'10), Cairo University, Egypt, December 19-21, 2010, Paper ID 160.

[24] McQuiston, F.C., Parker, J.D. and Spitler, J.D., 2000. Heating, Ventilating and Air-Conditioning: Analysis and Design. Fifth edition. John Wiley & Sons. Inc.